PHYSICAL REVIEW D VOLUME 32, NUMBER 4 15 AUGUST 1985

Membrane viewpoint on black holes: Dynamical electromagnetic fields near the horizon

Douglas A. Macdonald and Wai-Mo Suen
Theoretical Astrophysics and Gravitation, California Institute of Technology, Pasadena, California 91125
(Received 30 July 1984)

This paper is part of a series of papers with the aim of developing a complete self-consistent formalism for the treatment of electromagnetic and gravitational fields in the neighborhood of a black-hole horizon. In this *membrane* formalism, the horizon is treated as a closed two-dimensional membrane lying in a curved three-dimensional space, and endowed with familiar physical properties such as entropy and temperature, surface pressure and viscosity, and electrical conductivity, charge, and current. This paper develops the concept of the "stretched horizon," which will be vital for both the electromagnetic and gravitational aspects of the formalism, and it presents several model problems illustrating the interaction of dynamical electromagnetic fields with stationary black-hole horizons: The field of a test charge in various states of motion outside the Schwarzschild horizon is analyzed in the near-horizon limit, where the spatial curvature may be ignored and the metric may be approximated by that of Rindler. This analysis elucidates the influence of the horizon on the shapes and motions of electric and magnetic field lines when external agents move the field lines in arbitrary manners. It also illustrates how the field lines interact with the horizon's charge and current to produce an exchange of energy and momentum between the external agent and the horizon. A numerical calculation of the dynamical relaxation of a magnetic field threading a Schwarzschild black hole is also presented, illustrating the "cleaning" of a complicated field structure by a black-hole horizon, and elucidating the constraints on the location of the stretched horizon.

I. INTRODUCTION

During the 1970's theoretical studies of the physics of black holes showed that black-hole horizons behave as though they were endowed with various physical properties, including entropy and temperature,[1–5] surface pressure and viscosity,[6,7] and electric conductivity, charge, and current.[8–10] Motivated by these studies, in 1978 Damour[10] reformulated the standard theory of black-hole horizons in terms of precise boundary conditions which involve these horizon properties and others. (See also the independent, partial reformulation by Znajek.[8])

Damour's formalism is a powerful foundation on which to build a physically intuitive picture of black-hole physics. But it is only a partial foundation. An intuitive picture of black holes needs, in addition, an intuitively familiar formulation of the laws of physics for the surrounding spacetime, which may contain accretion disks, electromagnetic fields, orbiting stars, etc. The standard generally covariant laws of general relativity do not do the job; but if one performs on them a "3 + 1 split" (a split of spacetime into space plus time), they acquire an adequately intuitive form.

These considerations have led the authors and their Caltech colleagues to combine Damour's horizon formalism with a 3 + 1 split of the spacetime around a black hole, thereby obtaining a reformulation of the laws of physics which has intuitive appeal and power. Because this reformulation regards the horizon as a two-dimensional, membrane-like surface residing in a three-dimensional space (and evolving as time passes), we call it the "membrane formalism" for black holes.

Our membrane formalism is completely equivalent, mathematically, to the standard general relativistic black-hole formalism [see, for example, Chaps. 33 and 34 of Misner, Thorne, and Wheeler (MTW) (Ref. 11) and the theoretical sections of DeWitt and DeWitt[12]], but the mental and verbal pictures associated with the two formalisms are rather different. Our membrane studies (mostly not yet published) suggest that the standard formalism and pictures are the more powerful for studying highly dynamical black holes, but that the membrane formalism and pictures will be more powerful for studying complicated physics around slowly evolving holes. Thus, we regard the membrane formalism as a potentially powerful tool for theoretical astrophysics.

This is the third paper in our research group's series on the membrane formalism. Paper I, by Thorne and Macdonald,[13] constructed the 3 + 1 split of electromagnetic theory in an arbitrary curved spacetime; then it specialized the 3 + 1 electromagnetism to the spacetime outside a rotating black hole and there married it to Damour's horizon equations to give the electromagnetic portion of our membrane formalism. Paper II, by Macdonald and Thorne,[14] used this membrane formalism to analyze the structure of stationary, axisymmetric black-hole magnetospheres and to study the Blandford-Znajek[15] process, by which such magnetospheres may power quasars and active galactic nuclei.

In this third paper we turn from stationary electromagnetic fields outside black holes to dynamical electromagnetic fields. Our objective is to build up physical intuition by studying a number of idealized thought experiments in which dynamical fields interact with the horizon of a sta-

tionary black hole.

In future papers in this series, we and other members of our Caltech group will develop the membrane formulation of gravitational perturbations of a stationary black hole,[16] we will study idealized thought experiments which give physical insight into gravitational perturbations and their effects on the evolution of the hole,[17] and we will present a pedagogical review of the formalism and its insights.[18]

For the sake of brevity, we assume in this paper that the reader is fully familiar with general relativity theory, at least at the level of track 1 of MTW. However, our future review paper[18] will be written in a form understandable to people who have had only vague contacts with relativity theory.

The structure of this paper is as follows:

In Sec. II, we review the electromagnetic features of the membrane viewpoint and introduce the concept of the *stretched horizon,* which is fundamental to both the electromagnetic and the gravitational aspects of the membrane viewpoint.

In Sec. III, we study electromagnetic fields very near the horizon of a Schwarzschild black hole. We focus attention on a region close enough to the horizon that the curvature of space can be ignored. In this region, the Schwarzschild geometry may be approximated by the algebraically simpler Rindler[19] geometry. We derive the general solution of the electromagnetic field equations in Rindler spacetime and apply it to obtain the fields of charges in various states of motion near the hole's stretched horizon. Those fields (Figs. 3–9) give insight into the electromagnetic properties of the stretched horizon.

Section IV presents a numerical calculation modeling the fully dynamical evolution of a magnetic field in a Schwarzschild background (Figs. 10–12). This example illustrates the "cleaning" of a complicated electromagnetic field by a hole's stretched horizon and also elucidates the constraints on the amount of stretching one should do when passing from the true horizon to the stretched horizon.

Section V describes how the intuition gained from the model problems of Secs. III and IV can be used to understand heuristically other interactions of black holes with electromagnetic fields.

II. THE 3 + 1 FORMALISM AND THE STRETCHED HORIZON

In this section, we will briefly review the electromagnetic aspects of the membrane viewpoint, mainly in order to define terms and notation for later use. For further details and derivations, see Thorne and Macdonald[13] (henceforth denoted TM) and Macdonald and Thorne[14] (henceforth denoted MT).

In the 3 + 1 formalism, we choose a space-filling, rotation-free family of timelike fiducial observers (FIDO's), whose world lines cover the entire spacetime outside the black hole, and we regard the hypersurfaces orthogonal to their world lines as a curved, "absolute" three-dimensional space viewed at different moments of time. (The fact that the congruence is rotation-free guarantees the existence of these hypersurfaces.) We label the hypersurfaces with a parameter t, which we call "universal time." The relation between the proper time τ of the FIDO's and the universal time t is given by the lapse function

$$\alpha=\left.\frac{d\tau}{dt}\right|_{\text{along FIDO world line}} . \tag{2.1}$$

The negative four-acceleration of a FIDO $\mathbf{g}=-\nabla\ln\alpha$ lies in the absolute space and plays the role of the "gravitational acceleration measured by the FIDO." (Here and throughout, all vectors and vector operators, e.g., $\mathbf{g}$ and ∇, are three-dimensional and live in the absolute space.) The magnitude of $\mathbf{g}$ diverges at the horizon, but the "renormalized" quantity $\alpha\,|\,\mathbf{g}\,|$ has a finite limit at the horizon; this limit is the "surface gravity" g_H of the hole.

The electric and magnetic fields and the charge and current densities are defined physically by measurements made by the FIDO's. Mathematically this corresponds to the definition

$$\begin{aligned} &E^\alpha=F^{\alpha\beta}u_\beta\ ,\quad B^\alpha=-\tfrac{1}{2}\epsilon^{\alpha\beta\gamma\delta}u_\beta F_{\gamma\delta}\ ,\\ &\rho_e=-J^\alpha u_\alpha\ ,\quad j^\alpha=(g^{\alpha\beta}+u^\alpha u^\beta)J_\beta\ , \end{aligned} \tag{2.2}$$

where u^α is the FIDO four-velocity, $F^{\alpha\beta}$ is the Maxwell field tensor, and J^α is the four-current density. These E^α, B^α, ρ_e, and j^α are tangent to the hypersurfaces $t=$constant and thus live as three-vectors and scalars in absolute space. Using these electric and magnetic fields, the curved-space Maxwell equations take a form very similar to their flat-space analogs [see TM Eq. (3.4)].

The 3 + 1 formalism developed here will be most useful when a particular choice of fiducial observers is singled out by the geometry. For the problems we will study in this paper, namely, Schwarzschild black holes with dynamical electromagnetic "test" fields whose gravitational effects are ignored, such a preferred set of FIDO's is the set of "zero-angular-momentum observers," or ZAMO's.[20] With this choice, the global time parameter t is equal to the standard Schwarzschild time coordinate; the lapse function and the three-metric of absolute space have the form

$$\alpha=(1-2M/r)^{1/2}\ , \tag{2.3a}$$

$$ds^2=(1-2M/r)^{-1}dr^2+r^2(d\theta^2+\sin^2\theta d\phi^2)\ ; \tag{2.3b}$$

the horizon's surface gravity is

$$g_H=|\,\alpha\nabla\ln\alpha\,|_{\alpha=0}=1/4M\ ; \tag{2.3c}$$

and Maxwell's equations read

$$\begin{aligned} &\nabla\cdot\mathbf{E}=4\pi\rho_e\ ,\\ &\nabla\cdot\mathbf{B}=0\ ,\\ &\partial\mathbf{E}/\partial t=\nabla\times(\alpha\mathbf{B})-4\pi\alpha\mathbf{j}\ ,\\ &\partial\mathbf{B}/\partial t=-\nabla\times(\alpha\mathbf{E})\ , \end{aligned} \tag{2.3d}$$

where M is the mass of the black hole.

Since our absolute three-dimensional space covers only the exterior of the black hole, Maxwell's equations have to

be supplemented by a set of boundary conditions on the horizon, $\alpha=0$, namely the Znajek[8]-Damour[10] horizon equations (TM Sec. 5.4). In attempting to apply these boundary conditions, however, we come up against a pathology of the family of spacetime hypersurfaces $t=$constant in terms of which the $3+1$ split is made. Because the ZAMO world lines become null at the horizon, their orthogonal hypersurfaces also become null there; i.e., they coincide with the horizon as $\alpha\to 0$. They achieve this by extending deep into the past as they approach the horizon. This may be seen from Fig. 1, which shows the $t=$constant hypersurfaces plotted in spacetime as functions of the Eddington-Finkelstein time coordinate

$$\tilde{t}=t+2M\ln(r/2M-1)\ , \tag{2.4}$$

which is well-behaved at the horizon (cf. Box 31.2 of MTW). This ill behavior of the spatial hypersurfaces means that the ZAMO's will never see any infalling particle or any part of the electromagnetic field actually cross the horizon, but rather the ZAMO's will observe them asymptotically approach and hover just above the horizon. If the electromagnetic field is dynamical, the near-horizon fields will form a layered structure reflecting their entire past evolutionary history.

If one (mathematically) approaches the horizon along a particular $t=$constant hypersurface in order to try to define a horizon boundary condition at that moment of universal time t, one will not see the field settle down to a well-defined value which may be used as a boundary value. Rather, the field will point first one way, and then another, as one examines the relic fields reflecting more and more ancient eras of the near-horizon region.

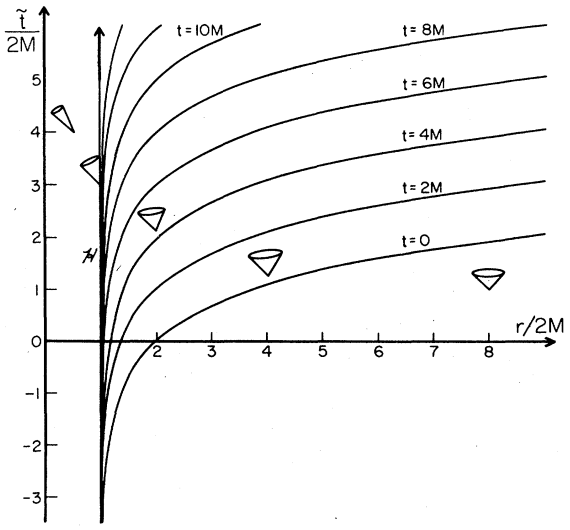

FIG. 1. The surfaces of constant universal time t around a Schwarzschild black hole, as viewed in Eddington-Finkelstein coordinates. The Eddington-Finkelstein time coordinate $\tilde{t}$ is related to universal time by $\tilde{t}=t+2M\ln(r/2M-1)$, and the Eddington-Finkelstein coordinate r is identical to the Schwarzschild r. The cones are the radial light cones as given by the metric in Eddington-Finkelstein coordinates:

$$ds^2=-d\tilde{t}^2+dr^2+(2M/r)(d\tilde{t}+dr)^2+r^2(d\theta^2+\sin^2\theta d\phi^2)\ .$$

A way of avoiding this difficulty in defining boundary conditions at the horizon was suggested briefly in TM, Sec. 5.3, but was not developed there. This method consists of choosing a closed two-dimensional surface just outside the horizon, and applying boundary conditions on this surface rather than on the true horizon. We will call this surface the *stretched horizon,* and for mathematical convenience[16] we will take it to have a fixed (time-independent and angle-independent) location $\alpha=\alpha_H\ll 1$.

By defining boundary conditions on the stretched horizon, we ignore the layered fossil field structure between the stretched horizon and the true horizon. Field boundary values defined at the stretched horizon differ from the values on the true horizon at the same moment of $\tilde{t}$ time by terms of order α_H, so boundary conditions posed on the stretched horizon become increasingly accurate as the stretched horizon is moved closer to the true horizon. In solving a particular problem, the stretched horizon must be chosen so that fractional errors of order α_H are small enough to be tolerated. It also of course must be chosen so that no interesting physics takes place between the stretched horizon and the true horizon.

One purpose of the model problems in this paper is to demonstrate the efficacy of the procedure of stretching the horizon and to determine what constraints exist on the choice of its position.

The "membrane" version of the true horizon's electromagnetic boundary conditions, without an external $3+1$ split, has been derived in elegant form by Znajek[8] and Damour.[9,10] Carter[21] reviews that formalism, and TM have translated it into $3+1$ language. Although the TM version is not expressed specifically in terms of a stretched horizon, it is trivial to show that when so expressed it takes the form described below.

The ZAMO-measured field components $\mathbf{E}_{||}$ and $\mathbf{B}_{||}$ parallel to the horizon diverge as α^{-1} when $\alpha\ll 1$. This is due to the fact that the ZAMO's are accelerating outward to keep from falling into the horizon; they are boosted to almost the speed of light $v\simeq 1$ relative to physically reasonable infalling observers, who see finite fields at the horizon. The horizon-parallel field seen by the ZAMO's thus diverges proportionally to the "gamma factor" $\gamma=(1-v^2)^{-1/2}\propto\alpha^{-1}$ of this boost, while the horizon-normal fields $E_n\equiv(\mathbf{E}\cdot\mathbf{n})_{\rm SH}$ and $B_n\equiv(\mathbf{B}\cdot\mathbf{n})_{\rm SH}$ remain finite. (Here $\mathbf{n}$ is the unit outward normal vector at the stretched horizon and the subscript SH denotes evaluation at the stretched horizon.) It is therefore convenient to define "renormalized" parallel fields on the stretched horizon

$$\begin{aligned}\mathbf{E}_H&\equiv(\alpha\mathbf{E}_{||})_{\rm SH}\ ,\\ \mathbf{B}_H&\equiv(\alpha\mathbf{B}_{||})_{\rm SH}\ .\end{aligned} \tag{2.5}$$

These renormalized fields have the advantage that they are nearly independent of the location chosen for the stretched horizon. They are equal, to within fractional errors of order α_H, to the true-horizon fields defined by Znajek, Damour, Carter, and MT. Since we will often have need of this concept, we will define the notation "$\cong$" to mean "equal, to within fractional terms of order α_H."

In terms of the horizon fields, one may define (imaginary) surface charge and current densities on the stretched horizon:

$$\sigma_H \equiv \frac{E_n}{4\pi} , \tag{2.6a}$$

$$\mathcal{J}_H \equiv \frac{1}{4\pi} \mathbf{n} \times \mathbf{B}_H . \tag{2.6b}$$

These definitions link the horizon charges and currents to the external fields in the way which would be expected from Gauss's and Ampere's laws. An observer falling through the horizon would not see a charge layer or current sheet on the horizon, of course, but the fields seen by observers who remain outside the hole (e.g., ZAMO's) are accounted for by imagining that the surface charge and current exist on the stretched horizon and ignoring all charge and current, as well as the normal electric field E_n and tangential magnetic field $\mathbf{B}_{||}$, inside the stretched horizon. For example, the stretched horizon of a Reissner-Nordström black hole with charge Q will have a uniform surface charge density Q/(surface area of stretched horizon) in the absence of external sources.

Znajek, Damour, Carter, and MT show that one of the standard black-hole-horizon boundary conditions translates into an Ohm's law:

$$\mathcal{J}_H \cong \frac{\mathbf{E}_H}{R_H} , \tag{2.7}$$

where $R_H \equiv 4\pi \simeq 377\ \Omega$ is the surface resistivity of the stretched horizon. Moreover, another of the standard boundary conditions translates into the statement that the horizon charge and current densities "close the circuit" of external currents entering the stretched horizon:

$$(\alpha j_n)_{\rm SH} \cong -\frac{\partial \sigma_H}{\partial t} - {}^{(2)}\nabla \cdot \mathcal{J}_H . \tag{2.8}$$

This equation says, more precisely, that whenever electric charge falls into the stretched horizon, it can be regarded as stopping its fall and thereafter moving around on the stretched horizon in a conserved manner, until such a time as it reemerges into the external universe (in the form of opposite charges moving inward, of course). The factor of α in Eq. (2.8) serves to renormalize $\mathbf{j}$, the current density measured by ZAMO's, from a "per-unit-ZAMO-proper-time τ" basis to a "per-unit-global-time t" basis—the same kind of time as is used in $\partial\sigma_H/\partial t$ and in $\mathcal{J}_H$.

Equations (2.6b) and (2.7) imply that

$$\mathbf{E}_H \cong \mathbf{n} \times \mathbf{B}_H , \tag{2.9}$$

i.e., the fields at the stretched horizon have the form of ingoing plane waves. This might have been expected from the fact that the horizon's surface resistivity $R_H = 4\pi$ is just the impedance of free space at the end of an open waveguide.

The horizon surface charges and currents enter into dynamical equations in the same way as do ordinary charges and currents. The rate of change of the horizon's momentum density (momentum per unit area) $\mathbf{\Pi}_H$ with respect to global time t, produced by an electromagnetic field, is given by the expected Lorentz-force law:[10,16]

$$\frac{d}{dt} \mathbf{\Pi}_H \cong \sigma_H \mathbf{E}_H + \mathcal{J}_H \times B_n \mathbf{n} . \tag{2.10}$$

[If the hole begins precisely nonrotating at $t=0$, then $\mathbf{\Pi}_H = 0$ at $t=0$ and a subsequent growth of $\mathbf{\Pi}_H$ corresponds to a gradual spin-up of the hole. For very slow rotation about the polar ($\theta=0$) axis, the total angular momentum is[10,21] $J = \int_{\rm SH} (\mathbf{\Pi}_H \cdot \partial/\partial\phi) dA \cong I_H \Omega_H$, where $I_H = 4M^3$ is a Schwarzschild hole's moment of inertia[22] and $\Omega_H \ll 1/M$ is the angular velocity.] The fields also increase the black hole's entropy (area) in accord with the Joule-heating relation[8,9]

$$T_H \frac{dS_H}{dt} \cong \int_{\rm SH} \mathcal{J}_H \cdot \mathbf{E}_H dA , \tag{2.11}$$

where T_H is the black hole's temperature and S_H is its entropy, and they increase its mass in accord with the first law of black-hole thermodynamics[23] $dM = T_H dS_H + \Omega_H dJ$ ($\simeq T_H dS_H$ for very slow rotation).

The use of "renormalized quantities" on the stretched horizon may generate some initial uneasiness. We have defined all physical quantities living in the absolute space in terms of ZAMO measurements, and we could equally well have used these ZAMO-defined fields ($\mathbf{E}$, $\mathbf{B}$, σ, and $\mathbf{j}$) in defining the boundary conditions on the stretched horizon, without the renormalization factor α_H. The advantage of such an approach would be the simplicity of using a single set of fields in our absolute space and on the stretched horizon; the disadvantage would be that the unrenormalized stretched-horizon fields would depend very sensitively on α_H, i.e., on the location chosen for the stretched horizon, and in general they would diverge as the stretched horizon approached the true horizon. Clearly, since α_H is chosen to be a constant throughout this work, all equations we write describing the physical properties of the stretched horizon and the relations between its various fields would be valid regardless of which convention was adopted. However, we will choose to present the horizon boundary conditions in terms of the renormalized field quantities in order to maintain notational consistency with papers I and II and also to enable the formalism to be generalized in our future papers to gravitational interactions with horizons.

The model problems in the following sections will illustrate the utility of the concept of the stretched horizon and will elucidate the constraints which exist on where it may be chosen (i.e., on the value of α_H), and will help the reader develop an intuitive feeling for the membrane view of black holes.

III. ELECTROMAGNETIC FIELDS OF POINT CHARGES NEAR A SCHWARZSCHILD BLACK HOLE

A. The Rindler approximation

In this section we focus our attention on the interaction of a black-hole horizon with the electromagnetic fields of point charges. In order to get maximum insight from a minimum of computational labor, we shall restrict attention to charges that are very close to the horizon and to the near-horizon fields that they produce. This permits us

to approximate the Schwarzschild spatial geometry and lapse function by those of Rindler, which cover only the near-horizon region $r-2M \ll 2M$ and ignore the spatial curvature there.

In the region near the horizon, the Schwarzschild spatial metric (2.3b) may be written in the form [cf. TM, Eq. (5.29)]

$$ds^2=d\alpha^2/g_H^2+(2M)^2(d\theta^2+\sin^2\theta d\phi^2) ,$$

where α is the lapse function and g_H is the surface gravity of the hole. If one restricts attention to a region of dimensions $\ll M$ centered on the location (θ_0,ϕ_0) on the horizon, and then defines the variables $x=2M\sin\theta_0(\phi-\phi_0)$, $y=2M(\theta-\theta_0)$, and $z=\alpha/g_H$, the lapse function and the metric take the Rindler[19] form

$$\alpha=g_H z , \quad ds^2=dx^2+dy^2+dz^2 . \tag{3.1}$$

The coordinates (t,x,y,z) will be called Rindler coordinates; in these coordinates the horizon is at $\alpha=z=0$. Therefore, the Rindler geometry can be considered as an approximation to the metric of a spherically symmetric black hole in the limit as one approaches the horizon. In the Rindler approximation, z is the proper distance from the horizon, and it is related to the usual Schwarzschild radial coordinate r by

$$\int_{2M}^{r} \frac{dr}{(1-2M/r)^{1/2}} \simeq 4M(1-2M/r)^{1/2}=\alpha/g_H=z . \tag{3.2}$$

Of course, in approximating Schwarzschild space by Rindler space, a certain amount of information is lost. The Rindler approximation neglects the spatial curvature near the horizon; it approximates the lapse function α as linear in the distance z from the horizon; and consequently it characterizes the black hole's gravitational field entirely by the gravitational acceleration $\mathbf{g}=-\nabla\ln\alpha=-(g_H/\alpha)\mathbf{e}_z$ felt by the ZAMO's. As a result, the Rindler approximation loses sight of the physics associated with spacetime curvature, such as the reflection of electromagnetic waves by the gravitational field, the "tails" of electromagnetic waves,[24] and the Smith-Will electrostatic self-force[25] on a charge in a curved background. Also, as we restrict ourselves to a region of space of dimensions much less than M, the global structure of the external electromagnetic field is lost.

But the Rindler approximation is nonetheless a valuable tool in studying electromagnetic fields near a black-hole horizon, since the gravitational acceleration $\mathbf{g}$ is the major influence on the near-horizon field structure of a Schwarzschild black hole. The Rindler approximation combines the kinematic properties of horizons predicted by the membrane formalism (such as electrical conductivity) with an algebraic simplicity lacking in full Schwarzschild. This simplicity permits us to obtain the general analytic solution of the electromagnetic field equations, and thus allows us to develop a detailed understanding of the physics associated with the presence of the horizon. In fact, this consideration is not restricted to electromagnetism; in a future paper, Suen, Price, and Redmount[17] will also use the Rindler approximation to study the gravitational aspects of the membrane viewpoint. It is also well known that Hawking radiation near a black-hole horizon may be understood in terms of the Rindler approximation's acceleration radiation.[26]

B. Solution of field equations in the Rindler approximation

In order to solve the curved-space Maxwell equations (2.3d) in the Rindler approximation, we note that, since Rindler spacetime is flat, it may be transformed to Minkowski-type coordinates (T,X,Y,Z):

$$T=z\sinh g_H t, \quad Z=z\cosh g_H t , \qquad X=x , \quad Y=y . \tag{3.3}$$

These coordinates are associated with a family of observers who are falling freely in the z direction, and who ultimately fall into the horizon. In terms of Minkowski coordinates, the four-metric associated with Eq. (3.1) is

$$\begin{aligned} {}^{(4)}ds^2 &= -\alpha^2 dt^2+dx^2+dy^2+dz^2 \\ &= -dT^2+dX^2+dY^2+dZ^2 . \end{aligned}$$

To solve for the general electromagnetic field, we will transform the Minkowski-spacetime Liénard-Wiechert potential[27] into Rindler coordinates.

We consider a charge Q moving with four-velocity $u^{\alpha'}(x)$ which is a function of spacetime position x. (Here primed letters will be taken to denote four-vector indices in Minkowski coordinates, while unprimed ones will denote four-indices in Rindler coordinates.) The electromagnetic four-potential $A^{\alpha'}(x)$ at a particular spacetime observation point x will be generated entirely by a single point of the charge's trajectory: the retarded point x_R which lies at the intersection of the particle's trajectory with the past null cone of the observation point. The Liénard-Wiechert potential is

$$A^{\alpha'}(x)=\frac{Qu_R^{\alpha'}}{u_{R\beta'}(x_R^{\beta'}-x^{\beta'})} , \tag{3.4}$$

where

$$|x_R^{\beta'}-x^{\beta'}| \equiv [(x_R^{\alpha'}-x^{\alpha'})(x_R^{\beta'}-x^{\beta'})\eta_{\alpha'\beta'}]^{1/2}=0$$

and where $\eta_{\alpha'\beta'}\equiv\mathrm{diag}[-1,1,1,1]$ are the Minkowski metric coefficients.

Transforming this expression to Rindler coordinates yields

$$A^{\alpha}(x)=L^{\alpha}_{O\alpha'}A^{\alpha'}=\frac{QL^{\alpha}_{O\alpha'}L^{\alpha'}_{R\beta}u_R^{\beta}}{u_{R\gamma}L^{\gamma}_{R\beta'}(x_R^{\beta'}-x^{\beta'})} , \tag{3.5}$$

where $L^{\alpha}{}_{\alpha'}\equiv\partial x^{\alpha}/\partial x^{\alpha'}$ and $L^{\beta'}{}_{\beta}\equiv\partial x^{\beta'}/\partial x^{\beta}$ are the transformation matrices between Rindler and Minkowski coordinates, the subscripts O and R denote evaluation at the observation point and retarded point, respectively, and $x^{\beta'}(x^{\beta})$ is given by Eq. (3.3). The factors of L_R appear in Eq. (3.5) because u_R^{α} is a vector at the retarded point x_R, not at the observation point.

In the numerator of Eq. (3.5), $L^{\alpha'}_{R\beta}u_R^{\beta}$ gives the Min-

kowski components $u_R^{\alpha'}$ of the retarded four-velocity. We parallel-transport it to the observation point by fixing its Minkowski components and then transform to Rindler coordinates using $L^{\alpha}_{O\alpha'}$. The factor $L^{\alpha}_{O\alpha'}L^{\alpha'}_{R\beta}$ is the bivector of geodetic parallel displacement defined by Dewitt and Brehme.[24] The potential (3.5) agrees with the Liénard-Wiechert potential given by Dewitt and Brehme as specialized to Rindler space.

Writing out Eq. (3.5) explicitly in terms of Rindler coordinates yields

$$\begin{bmatrix} A^t \\ A^x \\ A^y \\ A^z \end{bmatrix} = \frac{Q}{N} \begin{bmatrix} \frac{z_R}{z}\cosh g_H(t-t_R) & 0 & 0 & \frac{-1}{g_H z}\sinh g_H(t-t_R) \\ 0 & 1 & 0 & 0 \\ 0 & 0 & 1 & 0 \\ -g_H z_R \sinh g_H(t-t_R) & 0 & 0 & \cosh g_H(t-t_R) \end{bmatrix} \begin{bmatrix} u_R^t \\ u_R^x \\ u_R^y \\ u_R^z \end{bmatrix} , \tag{3.6a}$$

where

$$N \equiv g_H z z_R \sinh g_H(t-t_R)u_R^t - (z\cosh g_H(t-t_R) - z_R)u_R^z - (x-x_R)u_R^x - (y-y_R)u_R^y . \tag{3.6b}$$

The coordinates t_R, x_R, y_R, z_R of the retarded point are given in terms of those t,x,y,z of the field point by the intersection of the field point's past null cone

$$(x-x_R)^2+(y-y_R)^2+z^2+z_R^2-2zz_R\cosh g_H(t-t_R)=0 \quad (t_R<t) , \tag{3.7}$$

with the world line of the charge. Together, Eqs. (3.6), (3.7), and the particle's world line give the complete solution for the field of an arbitrarily moving charge in Rindler space. By linear superposition, we thereby know the general vector potential for an arbitrary distribution of charge and current.

In terms of the four-vector potential, the ZAMO-measured electric and magnetic fields (2.2) are [cf. MT Eq. (2.24)]

$$E^i = -\frac{1}{g_H z}[A^i_{,t} + (g_H^2 z^2 A^t)_{,i}] ,$$
$$B^i = \epsilon^{ijk}A_{k,j} , \tag{3.8}$$

where i,j,k run over x,y,z and ϵ^{ijk} is the three-dimensional alternating tensor.

In the following subsections, we will discuss the electromagnetic field structure generated by various source motions.

C. "Static" charge in Rindler space

For arbitrary motion of the source particle, it is generally not possible to solve Eq. (3.7) explicitly for the retarded coordinates as a function of the coordinates of the observation point. However, when the charged source particle is static in Rindler space, i.e., fixed at a position $(x,y,z)=(0,0,z_0)$, analytic expressions for the retarded coordinates may be derived and Eq. (3.6) may be used to write A^{α} solely in terms of the observer-point coordinates. In Fig. 2, the trajectory of the accelerated particle is plotted as a dashed line in both the Minkowski and Rindler spacetime coordinate systems.

Substituting $x_R=0$, $y_R=0$, and $z_R=z_0$ in Eq. (3.7) and adopting the cylindrical coordinates $\rho \equiv (x^2+y^2)^{1/2}$ and $\phi \equiv \tan^{-1}(y/x)$, we find

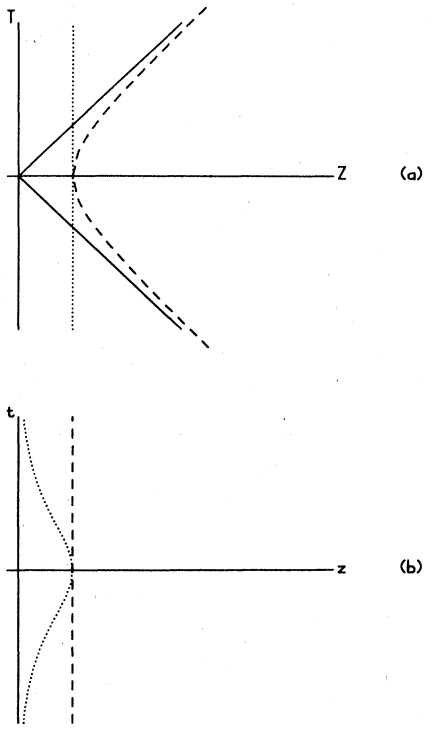

FIG. 2. The world lines of the Minkowski-stationary (dotted line) and Rindler-stationary (dashed line) charges, as seen in Minkowski (a) and Rindler (b) coordinates. The Minkowski-stationary charge is fixed at $Z=z_0$, while the Rindler-stationary charge is fixed at $z=z_0$. In diagram (a), the lower and upper 45° lines represent the past and future event horizons, respectively. In diagram (b), the intersection of the horizons is represented by the solid vertical line $z=0$, to which the dotted line asymptotes.

$$t_R = t - \frac{1}{g_H}\cosh^{-1}\left[\frac{z^2+\rho^2+z_0^2}{2zz_0}\right] . \tag{3.9}$$

Equation (3.6) then yields[28]

$$A^t = \frac{Q}{g_H z^2}\frac{z^2+\rho^2+z_0^2}{\xi} , \quad A^z = -\frac{Q}{z} ,$$
$$\xi \equiv [(z^2+\rho^2-z_0^2)^2+4\rho^2 z_0^2]^{1/2} . \tag{3.10}$$

From Eq. (3.8), the only nonvanishing physical components of the electromagnetic field are

$$E_\rho = \frac{8Qz_0^2\rho z}{\xi^3} ,$$
$$E_z = \frac{4Qz_0^2}{\xi^3}(z^2-\rho^2-z_0^2) . \tag{3.11}$$

As might be expected, this field is stationary in the sense

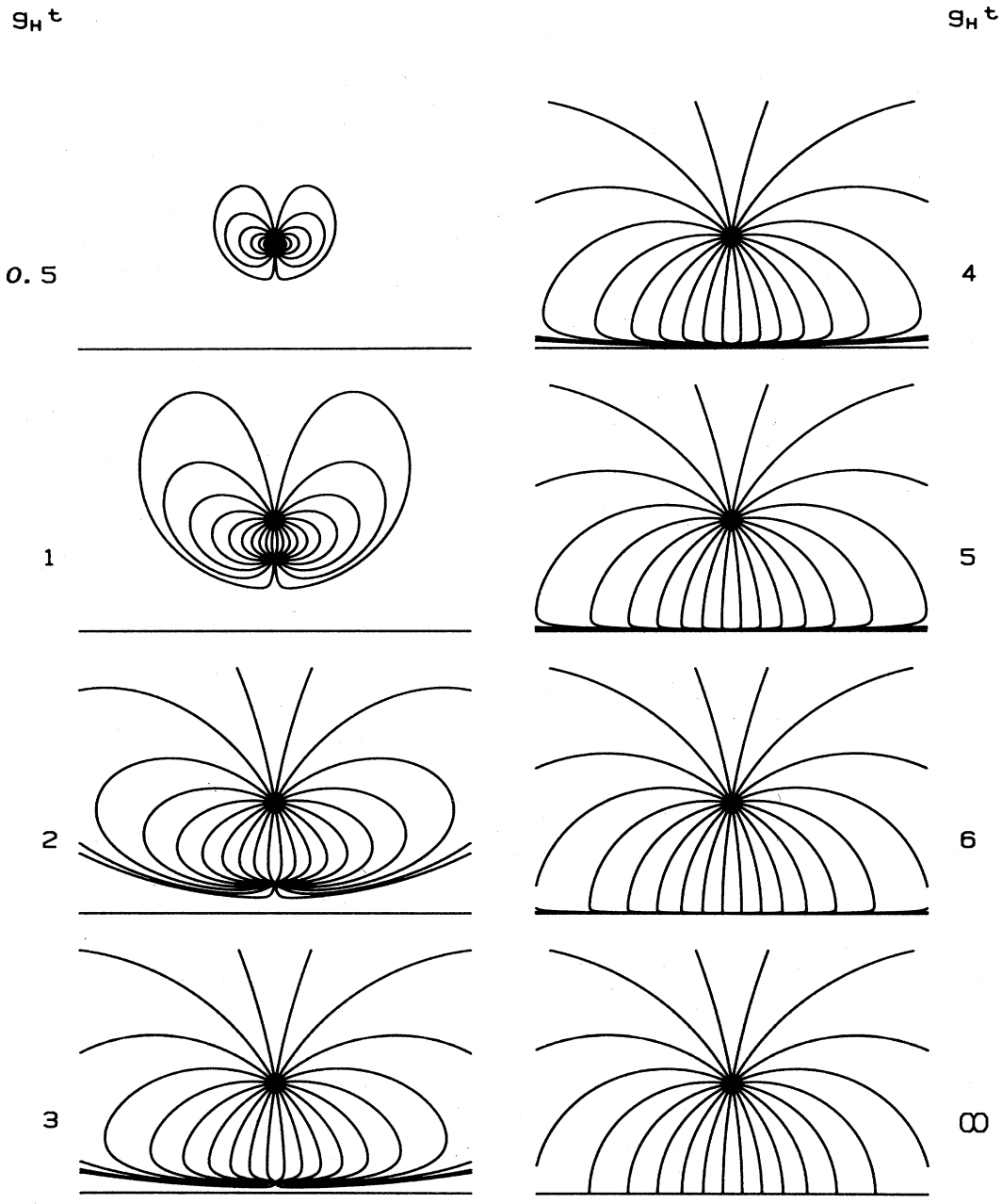

FIG. 3. Electric field lines for two opposite charges which split at $t=0$, $z=z_0$: one remaining stationary in Rindler coordinates, and the other stationary in Minkowski coordinates and thus falling into the horizon. The field-line diagrams are shown at different values of Rindler time t. By $t=6/g_H$, the field geometry has become almost indistinguishable from the field of the stationary charge alone, which is shown in the lower right-hand diagram.

that it does not depend on the Rindler time t and it is purely electric. It should also be noted that it is normal to the horizon at $z=0$. The electric field lines are plotted in the lower right corner of Fig. 3. It is a major advantage of the $3+1$ viewpoint that field lines may be used to describe the field. The Gaussian Maxwell equations $\nabla\cdot\mathbf{B}=0$ and $\nabla\cdot\mathbf{E}=4\pi\rho_e$ say, just as they do in flat-space electrodynamics, that magnetic field lines never end and that electric field lines end only on electric charge.

The horizon charge density Eq. (2.6a), which terminates the normal electric field of Eq. (3.11) at the horizon, is

$$\sigma_H=\left.\frac{E_z}{4\pi}\right|_{z=0}=-\frac{Qz_0^2}{\pi(\rho^2+z_0^2)^2}\ ; \tag{3.12}$$

and by integrating σ_H over the horizon, one can verify that the total charge induced on the horizon is equal to $-Q$. The horizon surface current density defined in Eq. (2.6b) vanishes, so there is no dissipation of energy in the horizon. The stretching of the horizon described in Sec. II is not necessary in this example since the field is stationary and therefore has none of the layered horizon-field structure described there.

It is important to note that, although the horizon surface charge density (3.12) was not explicitly included as a source in deriving the electric field (3.11) from Eqs. (3.6) and (3.8), its inclusion would not change the exterior field in any way. The reason for this is the defined role of the horizon surface charge: it terminates the normal electric field in the region exterior to the horizon, and annuls it in the interior region. Indeed, by substituting zero for z_0 in Eqs. (3.11), it may be seen that a hypothetical charge on the horizon $z=0$ produces no field in the exterior region. For the more general case (considered in the following sections) where the horizon must be stretched, the exterior fields produced by the induced charge and current densities on the stretched horizon may be shown to be of order α_H, the lapse-function value at the stretched horizon, and thus will vanish in the limit as the stretched horizon approaches the true horizon.

The same conclusion holds for a Schwarzschild black hole, which has zero net charge. As shown by Hanni and Ruffini,[29] a hypothetical charge on the horizon produces a radial electric field centered on the center of the hole. If the total charge on the horizon is zero, then no matter what its distribution, it will produce no external electric field. For a Reissner-Nordström black hole with total charge Q, the surface charge density σ_H consists of a total charge Q distributed over the horizon. Although this charge distribution may be distorted away from uniformity by the fields of external sources, the field generated by the horizon charge will remain the same as that of the Reissner-Nordström hole, i.e., $\mathbf{E}=Q/r^2$, $\mathbf{B}=0$.

The solution (3.11) might alternatively have been derived from the Copson-Linet[30] solution for a point charge at rest outside a Schwarzschild black hole by applying the change of variables and the limiting process (Rindler approximation) described in Eq. (3.2) and the preceding paragraph. The Copson-Linet solution is summarized in $3+1$ form in TM, Sec. 6.1; the field lines were first plotted by Hanni and Ruffini.[29] For a point charge Q at rest above the north pole of the hole at $r=b$, $\theta=0$, the horizon surface charge density for the Copson-Linet solution is [cf. TM Eq. (6.4)]

$$\sigma_H=\frac{Q[M(1+\cos^2\theta)-2(b-M)\cos\theta]}{8\pi b[b-M(1+\cos\theta)]^2}\ . \tag{3.13}$$

This charge density yields a total induced surface charge of zero. As shown in Fig. 6 of Ref. 29, the horizon is polarized, with a total charge $-2Q[b-M-\sqrt{b(b-2M)}]/b$ north of the critical colatitude

$$\theta=\theta_{\rm crit}\equiv\cos^{-1}\{[b-M-\sqrt{b(b-2M)}]/M\}\ ,$$

and a like charge of the opposite sign distributed south of this latitude. When one applies the Rindler approximation to Eq. (3.13), the critical radius where the sign of the polarization charge changes is moved out to $\rho=\infty$, so the charge density (3.12) is of the opposite sign to Q over the entire Rindler horizon.

Thus, we have verified that Eq. (3.6) gives the previously-known field of a Rindler-static charge; and we have shown explicitly that this field is a valid approximation to the field of a charge static outside Schwarzschild in the near-horizon limit. We now turn to the study of the fields of charges in motion above the Rindler horizon.

D. Infalling charge

Another simple source configuration which yields an explicit analytic solution for the fields is that of a charge $-Q$ stationary in Minkowski coordinates at position $Z=Z_0$, so that its trajectory in Rindler coordinates is

$$z=\frac{Z_0}{\cosh g_H t}\ . \tag{3.14}$$

As seen in Rindler coordinates, this particle emerges from the past horizon at $t=-\infty$, reaches a maximum distance Z_0 from it, and then falls into the future horizon at $t=+\infty$. In Fig. 2, the trajectory of this charge is shown as a dotted line in the two different coordinate systems. The physical components of the particle's field as seen by Minkowski observers (who are falling into the hole with the particle) are

$$E_{\rho'}=-\frac{Q\rho}{r^3}\ ,\quad E_{Z'}=-\frac{Q(Z-Z_0)}{r^3}\ , \tag{3.15}$$

where $r=[\rho^2+(Z-Z_0)^2]^{1/2}$. In Rindler coordinates the nonvanishing physical components are

$$\begin{aligned}E_\rho&=-\frac{Q\rho}{r^3}\cosh g_H t\ ,\\ E_z&=-\frac{Q}{r^3}(z\cosh g_H t-Z_0)\ ,\\ B_{\hat\phi}&=\frac{1}{\rho}B_\phi=\frac{Q\rho}{r^3}\sinh g_H t\ ,\end{aligned} \tag{3.16}$$

where

$$r\equiv[\rho^2+(z\cosh g_H t-Z_0)^2]^{1/2}$$

in terms of Rindler coordinates. These are the fields seen

by static observers (ZAMO's) outside the horizon, i.e., the fields which are used in our membrane viewpoint of black holes.

The definition of the horizon charge and current densities in this case is trickier than in the case of the Rindler-stationary charge. In attempting to calculate them, one evaluates E_ρ and E_z at the horizon ($z=0$, $t=\infty$), which leads to indeterminate results. The reason for this is the infinite gravitational red-shift at the horizon. As described in Sec. II, the field structure associated with the infalling charge only asymptotically approaches the horizon, and the tangential field strength at $z=0$ diverges exponentially with universal time t. To get meaningful results, it is necessary to define the charge and current densities on a stretched horizon as discussed in Sec. II. We choose it at the location $\alpha=\alpha_H \ll 1$, or $z=z_H \equiv \alpha_H/g_H$, where $0<z_H \ll Z_0$. The charge and current densities on the stretched horizon produced by the infalling charge are

$$\sigma_H = \frac{E_z}{4\pi}\bigg|_{z=z_H} = \frac{-Q(z_H \cosh g_H t - Z_0)}{4\pi[\rho^2+(z_H\cosh g_H t - Z_0)^2]^{3/2}} ,$$
$$\mathcal{J}_H = \left[\frac{\alpha}{4\pi}\mathbf{e}_z \times \mathbf{B}_{||}\right]_{z=z_H} = \frac{-Q g_H \rho z_H \sinh g_H t}{4\pi[\rho^2+(z_H\cosh g_H t - Z_0)^2]^{3/2}}\mathbf{e}_\rho , \tag{3.17}$$

respectively, where $\mathbf{B}_{||}$ is the component of $\mathbf{B}$ parallel to the horizon. As the particle descends toward the stretched horizon, the charge density becomes more and more sharply peaked at the position $\rho=0$ directly under the particle; the integral of σ_H over the stretched horizon, however, remains constant at the value $Q/2$ during the descent. In the limit as the particle approaches the stretched horizon, the charge density approaches the functional form

$$\sigma_H \to \frac{Q\delta(\rho)}{4\pi\rho} . \tag{3.18}$$

The surface current density feeds the growing concentration of charge at $\rho=0$.

As in the case of the Rindler-stationary charge treated in Sec. III C, the present problem is the near-horizon limit of a Schwarzschild problem: that of a charge which emerges from the horizon and falls back into it. As before, the charge simply polarizes the surface of the Schwarzschild hole, leaving it with zero net charge; but the Rindler approximation moves the neutral point where the polarization charge changes sign out to $\rho=\infty$, so that the charge density on the entire stretched Rindler horizon has the opposite sign to Q.

According to Eq. (2.11), the rate that energy is dissipated in a unit area of the stretched horizon is just $\mathcal{J}_H \cdot \mathbf{E}_H$, and the rate of increase of the hole's mass energy may be obtained by integrating this quantity over the stretched horizon:

$$\frac{dM}{dt} = T_H \frac{dS_H}{dt} \cong \int_{SH} \mathcal{J}_H \cdot \mathbf{E}_H dA = \frac{Q^2 g_H^2 z_H^2 \sinh g_H t \cosh g_H t}{8(z_H \cosh g_H t - Z_0)^2} . \tag{3.19}$$

The integral of this function over time, which should give the total mass energy absorbed by the horizon, diverges due to an infinite contribution at the point at which the particle crosses the stretched horizon. This is not unexpected, however, since the particle is assumed to be point-like and thus has an infinite amount of energy in its near field.

In contrast to the case of the Rindler-stationary charge, only half of the field lines of the infalling charge intersect the stretched horizon; the rest extend to spatial infinity. It may be seen by comparing Eqs. (3.14) and (3.16) that the electric field lines in Rindler coordinates emanate radially from the charge, just as they do in Minkowski coordinates. But unlike in Minkowski space, the field lines in Rindler space do not emerge from the charge isotropically. As the particle falls in, its field lines (even the ones that eventually extend to spatial infinity), are flattened down near the horizon within an ever-widening circle of radius $\Delta\rho \sim z_H \cosh g_H t$ on the stretched horizon. If its electric field lines were plotted, the entire field out to any chosen radius ρ would ultimately seem to disappear beneath the stretched horizon. Therefore, in plotting the field, it is convenient to add an oppositely charged particle, stationary outside the horizon, with field given by Eq. (3.11), to "hold the field lines up" and to illustrate the approach of the field toward stationarity.

Since we are considering Rindler space as an approximation to Schwarzschild, it is not physically realistic to consider the full trajectory of the Minkowski-stationary particle. Although the full analytic continuation of the Schwarzschild geometry has a past horizon, an astrophysical black hole does not. Therefore, we choose to consider the example of a neutral particle which splits into two parts at $t=0$, $z=z_0$: a charge $+Q$ which continues along the uniformly accelerated trajectory $z=z_0$, and a charge $-Q$ which falls freely into the hole along the trajectory $Z=z_0$. Thus, we set $Z_0=z_0$ in Eqs. (3.16) and then superpose the fields (3.11) and (3.16). The electromagnetic field will be given by this superposition inside the future light cone of the spacetime point $(t,x,y,z)=(0,0,0,z_0)$, and will vanish outside it. Likewise, the surface currents and charges (3.12) and (3.17) are valid at points on the stretched horizon within the future light cone of the splitting point, and vanish outside it. That is, currents flow only within the ever-widening circle

$$\rho = (2z_H z_0 \cosh g_H t - z_H^2 - z_0^2)^{1/2}$$

on the stretched horizon. If the charge densities corre-

sponding to the static and infalling particles are summed and integrated over this circle on the stretched horizon, it may be verified explicitly that the resulting total charge has the expected behavior: it vanishes for time $t<g_H^{-1}\cosh^{-1}(z_0/z_H)$ when the infalling charge is still above the stretched horizon, and is equal to $-Q$ after the charge falls through the stretched horizon.

Figure 3 shows the electric field lines resulting from this superposition at several representative times. It may be seen that the effects of the field of the infalling particle rapidly vanish, and that by about $t=6/g_H$, the field has very nearly settled down to the stationary form which would be produced by the static charge alone. All of the effects of the infalling particle's field become flattened into a thin layer just above the true horizon, the thickness of which decreases at a rate proportional to $1/\cosh g_H t \sim e^{-g_H t}$; thus all effects of the infalling charge disappear beneath the stretched horizon in a time of order $g_H^{-1}\ln(z_0/z_H)$.

E. Charge in uniform motion parallel to the horizon

In this subsection, we shall study the case of a charge sliding at constant height and with constant velocity above the Rindler horizon. We will analyze in detail the electric and magnetic fields, the work done on the charge, and the horizon heating.

We consider a charge Q which is located at $(x,y,z)=(0,0,z_0)$ at $t=0$ and which moves in the $+x$ direction with constant velocity $d\mathbf{x}/d\tau\equiv\mathbf{v}=\beta\mathbf{e}_x$, as seen by the ZAMO's, for all time $-\infty<t<\infty$. Thus, its velocity with respect to universal time t is $d\mathbf{x}/dt=\alpha\mathbf{v}=g_H z_0\beta\mathbf{e}_x$. If we set $\alpha_0\equiv g_H z_0$ and

$$x_R^\alpha=(t_R,\alpha_0\beta t_R,0,z_0)\ ,\qquad u_R^\alpha=(\gamma/\alpha_0,\ \gamma\beta,0,0)\ , \tag{3.20}$$

where $\gamma\equiv(1-\beta^2)^{-1/2}$, then Eqs. (3.6) and (3.8) yield

$$\begin{aligned}
E_x&=\frac{Q\gamma^3 z_0}{N^3}[D(\tilde\alpha+\beta SD-\beta^2 C)+\beta S(\beta^2-\tilde\alpha C)]\ ,\\
E_y&=\frac{Q\gamma^3 z_0}{N^3}\tilde y(\tilde\alpha+\beta SD-\beta^2 C)\ ,\\
E_z&=\frac{Q\gamma^3 z_0}{N^3}[\tilde\alpha\beta SD-(1+\beta^2)\tilde\alpha C+\tilde\alpha^2+\beta^2]\ ,\\
B_x&=\frac{Q\gamma^3 z_0}{N^3}\beta\tilde y(CD-\beta S)\ ,\\
B_y&=\frac{Q\gamma^3 z_0}{N^3}\beta[\beta SD-CD^2-C(\tilde\alpha^2+\beta^2)+\tilde\alpha(C^2+\beta^2)]\ ,\\
B_z&=\frac{Q\gamma^3 z_0}{N^3}\beta\tilde y(\tilde\alpha C-\beta^2)\ ,
\end{aligned} \tag{3.21}$$

where we have used coordinates normalized by z_0: $\tilde y\equiv y/z_0$, $\tilde\alpha\equiv\alpha/\alpha_0=z/z_0$, and a "lagging-comoving" x coordinate: $\tilde x\equiv x/z_0-g_H\beta t-\beta\ln(z/z_0)$. We also define

$$D\equiv(x-x_R)/z_0=\tilde x+\beta\ln[\tilde\alpha(C+S)]\ ,$$

where

$$C\equiv\cosh g_H(t-t_R)=(\tilde\rho^2+\tilde\alpha^2+1)/2\tilde\alpha\ ,$$

$$S\equiv\sinh g_H(t-t_R)=[(C^2-1)]^{1/2}\ ,$$

and $\tilde\rho^2\equiv D^2+\tilde y^2$. The quantity N of Eq. (3.6b) can be expressed as

$$N=\gamma z_0(\tilde\alpha S-\beta\{\tilde x+\beta\ln[\tilde\alpha(C+S)]\})\ .$$

Note that $\tilde\rho^2$ is defined implicitly in terms of the observer-point coordinates through C and S; only in the limit $\beta\to0$ can it be expressed explicitly as $\tilde\rho^2=\tilde x^2+\tilde y^2$, and thus only in this limit can the electric and magnetic fields be expressed completely explicitly in terms of the observer-point coordinates.

Figure 4(a) shows the electric field lines in the $x-z$ plane for a charge moving with $\beta=0.5$. Figure 4(b) shows a similar plot for the case $\beta=0.1$. In the region close to the charge, the electric field lines go out radially with an excess concentration factor γ in directions perpendicular to the motion, just as for a uniformly moving charge in Minkowski space. For $\beta=0.1$, the field structure resembles that of the Rindler-static charge (last diagram of Fig. 3) in a large region around the charge.

In the region close to the horizon, both the $\beta=0.1$ and $\beta=0.5$ cases show a similar tangential structure with

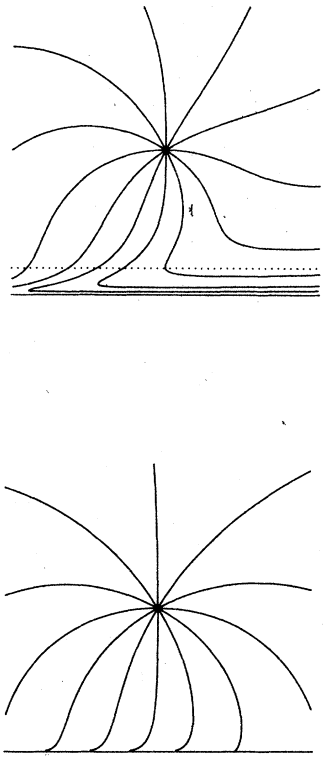

FIG. 4. Electric field lines in the x-z plane for a charge moving with uniform velocity $\beta\mathbf{e}_x$ in the $+x$ direction in Rindler space at a distance z_0 above the horizon. Part (a) shows the field lines for $\beta=0.5$. A possible choice of the stretched horizon is shown as a dotted line. Part (b) shows the field lines for the case $\beta=0.1$.

diverging tangential field strength, although the $\beta=0.1$ case shows this structure much closer to the horizon, so close that it cannot be resolved in the figure. The field in the tangential structure is complicated, varying rapidly in strength and direction as a function of α near the horizon. But any field line followed far enough toward the horizon will eventually point in the $+x$ direction, essentially because this part of the field was generated by the charge at early times when it was far to the left in the figure. Near the horizon, the tangential field structure is sinking slowly down toward the horizon at a rate $dz/dt=\alpha$, i.e., it is approaching the horizon asymptotically along the trajectory $z=\text{const}\times e^{-g_H t}$. (Note that the descent is slow relative to universal time t, but at the speed of light as measured locally by the ZAMO's.) The separation between neighboring field lines goes as α and the field-line density as measured by the ZAMO's thus diverges as α^{-1}, indicating a diverging tangential field strength near the horizon. However, the details of this near-horizon tangential field have no effect on the structure of the external field and thus may be conveniently ignored by stretching the horizon. A possible choice of the stretched horizon is shown as a dotted line in Fig. 4(a).

It may be seen from Fig. 4 that the largest normal field at the stretched horizon, and thus the largest concentration of horizon surface charge (2.6a), occurs at a position lagging behind the charge. The tangential fields drive a surface current (2.6b), which moves the surface charge concentration along the stretched horizon at a constant distance behind the charge. By evaluating E_z from (3.21), taking α_H to be small, and using Eq. (2.6a), we find the induced charge density on the stretched horizon to be

$$\sigma_H=\left.\frac{E_z}{4\pi}\right|_{\rm SH}=-\frac{Q}{\pi z_0^2}\frac{\tilde\rho^2+1+(\tilde\rho^2-1)\beta^2-(\tilde\rho^2+1)\beta D}{(\tilde\rho^2+1-2\beta D)^3}\ , \tag{3.22}$$

where $\tilde\rho$ is given implicitly by $\tilde\rho^2=D^2+\tilde y^2$, $D=\tilde x+\beta\ln(\tilde\rho^2+1)$. When $\beta=0$, this is easily seen to reduce to the static form Eq. (3.12). The variation of the charge density (3.22) along the x axis is shown in Fig. 5 for two different choices of stretched-horizon location: $\alpha_H^{(1)}=10^{-2}\alpha_0$ and $\alpha_H^{(2)}=10^{-4}\alpha_0$. It may be seen that in each case the charge is concentrated around $\tilde x=0$, i.e.,

$$x=x^*\equiv\alpha_0\beta t+(\alpha_0\beta/g_H)\ln(\alpha_H/\alpha_0)\ .$$

The quantity

$$\alpha_0\beta t-x^*=(\alpha_0\beta/g_H)\ln(\alpha_0/\alpha_H)$$

is the amount by which the induced charge distribution lags behind the source; it is given by the velocity of the source multiplied by the time required for the field to propagate from the position of the charge down to the stretched horizon. The size of the lag increases as α_H is made smaller, i.e., as the stretched horizon is moved closer to the true horizon. The qualitative features on the stretched horizon are independent of the value of α_H we choose (see also Fig. 6). They are just shifted in the x direction by an amount $(\beta/g_H)\ln(\alpha_H^{(1)}/\alpha_H^{(2)})$, since the field at $\alpha_H^{(2)}$ is laid down a time $(1/g_H)\ln(\alpha_H^{(1)}/\alpha_H^{(2)})$ earlier than the corresponding field on $\alpha_H^{(1)}$. As was stressed in Sec. II, we look at earlier epochs in the history of the field evolution as we look closer to the true horizon. We can understand the lag physically either by saying that there are strong retardation effects near the stretched horizon, or by noting that the stretched horizon has a finite resistivity which gives rise to a frictional force on the moving induced charges. This behavior is qualitatively the same as for the flat-space case of an external charge moving past a conducting surface with finite resistivity and dragging its induced charge behind itself.

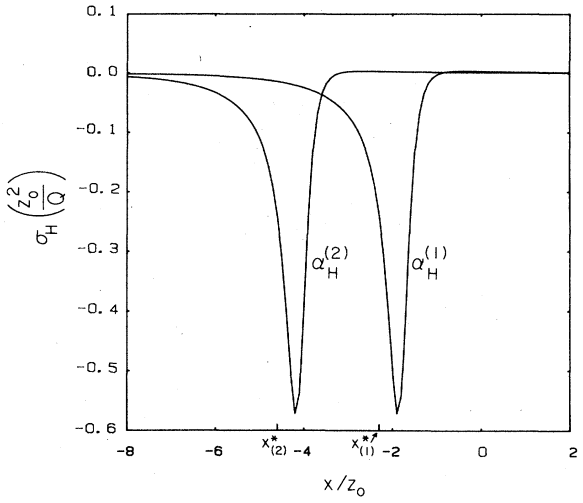

FIG. 5. The stretched-horizon surface charge density $\sigma_H(x,0,0)$ along the x axis (directly below the track of the particle), as induced by a charged particle in uniform motion parallel to the horizon at a height z_0 above it [same particle as in Fig. 4(a)]. The charge density is plotted in units of Q/z_0^2 and is shown for two different choices of stretched horizon location: $\alpha_H^{(1)}=10^{-2}\alpha_0$ and $\alpha_H^{(2)}=10^{-4}\alpha_0$. Both are shown at time $t=0$ for $\beta=0.5$. The points marked x^* are defined by $x^*=(\alpha_0\beta/g_H)\ln(\alpha_H/\alpha_0)$. Both plots go slightly positive in the region to the right of their large negative peaks.

Substituting the tangential electric field given by Eq. (3.21) into the definition (2.6b), we obtain the induced surface current density

$$\mathcal{J}_x=-\left.\frac{\alpha_H B_y}{4\pi}\right|_{\rm SH}=\frac{Q\alpha_0}{2\pi z_0^2}\frac{\beta(\tilde\rho^2+1)[2D^2-2\beta D+2\beta^2-(\tilde\rho^2+1)]}{(\tilde\rho^2+1-2\beta D)^3}\ , \tag{3.23}$$

$$\mathcal{J}_y = \frac{\alpha_H B_x}{4\pi}\bigg|_{\rm SH} = \frac{Q\alpha_0}{\pi z_0^2}\frac{\beta\tilde{y}(\tilde{\rho}^2+1)(D-\beta)}{(\tilde{\rho}^2+1-2\beta D)^3} .$$

Equations (3.22) and (3.23) can be combined to verify that

$$^{(2)}\nabla\cdot\mathcal{J}+\frac{\partial\sigma_H}{\partial t}=0 ,$$

which is the charge conservation equation, as there is no external charge entering the stretched horizon. This current distribution is shown in Fig. 6 for $\beta=0.5$, $t=0$, with $\alpha_H^{(1)}=10^{-2}\alpha_0$ and $\alpha_H^{(2)}=10^{-4}\alpha_0$.

The distribution of induced charge and current gives us immediate information on the energy and momentum transfer between the hole and the charge. The direction of the momentum transfer is evident from the fact that the induced charges on the stretched horizon suffer an Ohmic resistance as they move in the $+x$ direction; thus, momentum in the $+x$ direction will be transferred to the hole. Also, from Eq. (2.11), Joule heating of the horizon dissipates the Maxwell field energy at the rate

$$\frac{dM}{dt}=T_H\frac{dS_H}{dt}\cong\int_{\rm SH}\mathcal{J}_H\cdot\mathbf{E}_H dA . \tag{3.24}$$

Using the definitions (2.5) and (2.6) along with Ohm's law (2.7) and the zero-reflection boundary condition (2.9), this may be written as

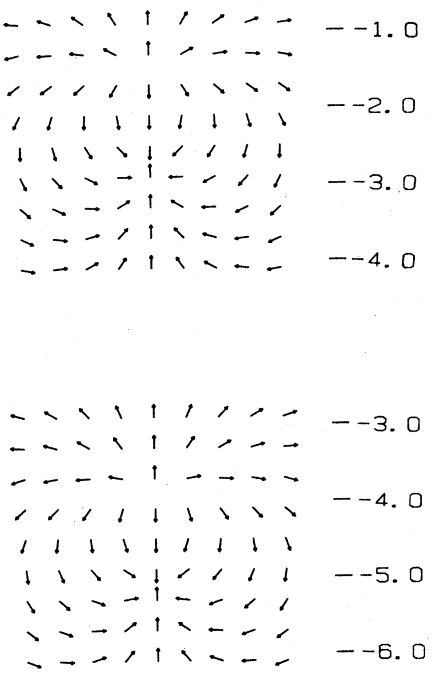

FIG. 6. The stretched-horizon surface current density induced by the moving charged particle of Figs. 4(a) and 5 for $\beta=0.5$, $t=0$. Part (a) shows the distribution on a stretched horizon at $\alpha_H^{(1)}=10^{-2}\alpha_0$, and part (b) for $\alpha_H^{(2)}=10^{-4}\alpha_0$. Values of x/z_0 are indicated by the scale next to each figure, showing that the lag of the current distribution increases as α_H is made smaller.

$$\frac{dM}{dt}\cong\alpha_H^2 F_E=\alpha_H^3\int_{\rm SH}T^{tz}dx\,dy , \tag{3.25}$$

where F_E is the ZAMO-measured energy flux into the stretched horizon and where one factor of α_H multiplying it comes from converting $d/d\tau$ to d/dt on the stretched horizon, and the other comes from red-shifting the energy. The Maxwell energy flux density in the z direction measured by ZAMO's on the stretched horizon is given by $\alpha_H T^{tz}=\alpha_H(E_yB_x-E_xB_y)/4\pi$. The heating rate dM/dt could be found explicitly by substituting the fields from Eq. (3.21) into Eq. (3.25) and performing the integration. However, it may be found much more easily by the following consideration.

The field energy dissipated in the horizon must be provided by the agent which keeps the charge in uniform motion. By considering the power supplied to the charge as measured by the local ZAMO at the position of the charge, the power flowing into the horizon can be easily evaluated (see the Appendix) to be

$$\frac{dM}{dt}=\tfrac{2}{3}Q^2g_H^2\frac{\beta^2}{(1-\beta^2)^2} . \tag{3.26}$$

Next we look at the momentum transfer between the charge and the horizon. In the membrane language, the momentum transfer is produced by a frictional force on the flowing induced charge in the stretched horizon; from Eq. (2.10) the x component of this force is

$$\frac{dp_H^x}{dt}\cong\int_{\rm SH}(\sigma_H\mathbf{E}_H+\mathcal{J}_H\times B_n\mathbf{n})_x dA . \tag{3.27}$$

Thus, from Eqs. (2.5) and (2.6), the torque on a Schwarzschild hole due to a charge moving in the ϕ direction at polar angle $\theta=\theta_0$, very close to the horizon, is

$$\frac{dJ}{dt}\cong 2M\sin\theta_0\frac{dp_H^x}{dt}=-2M\alpha_H\sin\theta_0\int_{\rm SH}T^{xz}dx\,dy , \tag{3.28}$$

where $2M\sin\theta_0$ is the "lever arm" for converting force to torque, and where

$$\alpha_H T^{xz}=-\alpha_H(E_xE_z+B_xB_z)/4\pi$$

is the Maxwell flux density of x momentum in the z direction, as measured by ZAMO's on the stretched horizon. The torque dJ/dt can be evaluated either by computing T^{xz} from Eqs. (3.21) for $\mathbf{E}$ and $\mathbf{B}$ and then performing the surface integration (3.28), or by the following consideration.

The momentum imparted to the horizon must be supplied by the agent which keeps the charge in uniform motion; in the Appendix, by computing the force on the charge, we obtain

$$\frac{dJ}{dt}=(2M\sin\theta_0)\frac{2}{3}\frac{Q^2g_H^2}{\alpha_0}\frac{\beta}{(1-\beta^2)^2} . \tag{3.29}$$

Note that since (power supply)$=\beta$(momentum supply), as measured by the ZAMO's at the position of the charge, then dJ/dt and dM/dt are very simply related:

$$dM/dt=\alpha_0\beta(2M\sin\theta_0)^{-1}dJ/dt .$$

It is also informative to look at the actual distribution of energy and momentum inflow on the stretched horizon, as given by T^{tz} and T^{xz} [cf. Eqs. (3.25) and (3.28)]. Figure 7 shows these distributions along the x axis, after integration over all y values. As may be readily seen by comparing Fig. 7 to Figs. 5 and 6, the region of greatest energy and momentum inflow coincides with the region of strongest induced charge and current.

Figure 7 shows that, from the viewpoint of our membrane formalism, the region of maximum inflow of energy and momentum lags behind the motion of the charge above the horizon. The question of whether this region lags or leads the charge is not completely unambiguous, however. It has been pointed out by Hartle[7] that an alternative, natural way to compare the transverse positions of points at different values of α (different distances from the horizon) is by means of a zero-angular-momentum light ray. This corresponds to a slicing of spacetime different from our choice: A coordinate change $\tilde{t}=t+(1/g_H)\ln\alpha$ brings the spacetime metric into the form

$$ds^2=-\alpha^2 d\tilde{t}^2+2\alpha\, d\tilde{t}\, dz+dx^2+dy^2 . \tag{3.30}$$

[The coordinate $\tilde{t}$ and the Minkowski time coordinate T are the Rindler-approximation limits of the infalling Eddington-Finkelstein time coordinate, Eq. (2.4), and the Kruskal-type time coordinate

$$4M(r/2M-1)^{1/2}\sinh(t/4M) ,$$

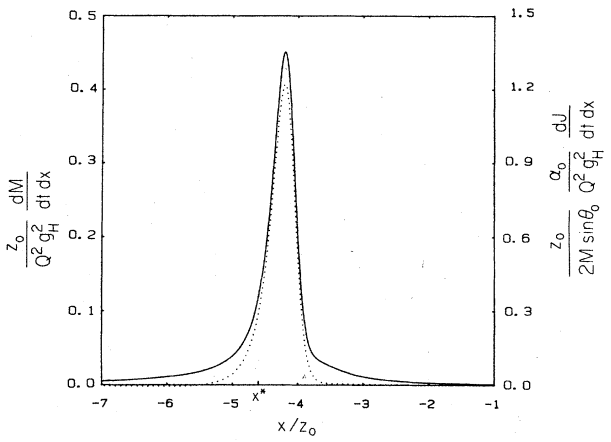

FIG. 7. The flux of energy and angular momentum carried into the stretched horizon by the electromagnetic field of the charged particle of Figs. 4(a), 5, and 6. The solid line (scale on left) shows the energy flux per unit x length $(1/Q^2g_H^2)(dM/dt\,dx)$ into the stretched horizon as a function of x, obtained by integrating the energy flux density over y. The dotted line (scale on right) shows the flux of x momentum per unit x length $(1/2M\sin\theta_0)(\alpha_0/Q^2g_H^2)(dJ/dt\,dx)$ into the stretched horizon. Both are shown at time $t=0$ for the choice of parameters $\beta=0.5$ and $\alpha_H=10^{-4}\alpha_0$ and both are plotted in units of z_0^{-1}. The point labeled x^* is the location where a zero-angular-momentum light ray from the charge's retarded position strikes the stretched horizon: $x^*=\beta z_0\ln(\alpha_H/\alpha_0)=-4.6z_0$. The momentum plot goes slightly negative in the region to the left of the peak.

respectively.] In the metric (3.30), a zero-angular-momentum null ray has the trajectory $\tilde{t}=$const, $x=$const, $y=$const, and hence, in a constant-$\tilde{t}$ slice, a zero-angular-momentum null ray starting from the charge will strike the stretched horizon directly underneath it. Such a position, after transforming back to the membrane viewpoint's t slicing, is marked as x^* in Fig. 7. We can clearly see that, from the "zero-angular-momentum-light-ray viewpoint," the location of maximum input of energy and momentum occurs at a position on the stretched horizon where the charge is not yet "overhead." The same kind of phase-lead phenomenon was observed by Hartle[7] when he studied the tidal bulge on the horizon due to an orbiting moon. However, when observed in a slice of constant t (the absolute space of our membrane viewpoint), the position of maximum energy and momentum input (or tidal bulge) will lag behind the source on the stretched horizon, which is much more suggestive to physical intuition.

F. Charge in nonuniform motion near the horizon

To obtain a better feeling for the evolution of field lines near the horizon, we consider charges that move only for a finite period of time.

We first consider a charge which stays at $(x,y,z)=(0,0,z_0)$ for all $t<0$, then moves with constant velocity $dx/d\tau=\alpha_0^{-1}dx/dt=\beta$ in the $\mathbf{e}_x$ direction until $t=1/g_H=z_0/\alpha_0$, and then stops again for all $t>1/g_H$ at $x=\beta z_0$. (We again set $\alpha_0\equiv g_H z_0$.) For $t>1/g_H$, the structure of the electric field lines is divided into three regions. Figure 8(a) shows the field lines for $t=2/g_H$, $\beta=0.5$. Near the charge there is a region centered at $x=\beta z_0$, $y=0$ where the field configuration has settled down to the static Coulomb field. In the region far away from the charge, we also have a static Coulomb field. This is the region where the charge's "start-to-move" signal has not yet arrived, i.e., the region where the spacetime separation from the point $t=0$, $x=0$, $y=0$, $z=z_0$ is space-like. Sandwiched between the near and far zones is the transition region, where the field is given by Eq. (3.21). (We idealize the charge's acceleration as being instantaneous and ignore the field generated at these instants. If this assumption were not made, there would be two shells of radiative field corresponding to retarded times during which the particle was accelerated. But the same conclusions would apply to these shells as to the transition region, so we will not consider them here.) As time progresses [Fig. 8(b)], those parts of the transition region propagating towards the horizon approach it asymptotically along a trajectory $z=\text{const}\times e^{-g_H t}$. Hence the transition region gets thinner and the field lines become more and more tangential. The field-line density increases as $1/\alpha$ and hence the tangential electric field grows. This tangential structure finally sinks down to the stretched horizon and drives a current which transports the surface charge from the region near $x=0$ to the region under the source's new position. There is also some surface charge attracted in from the region $x\gg 0$ to settle under the charge, while some excess charge near $x=0$ flows off in

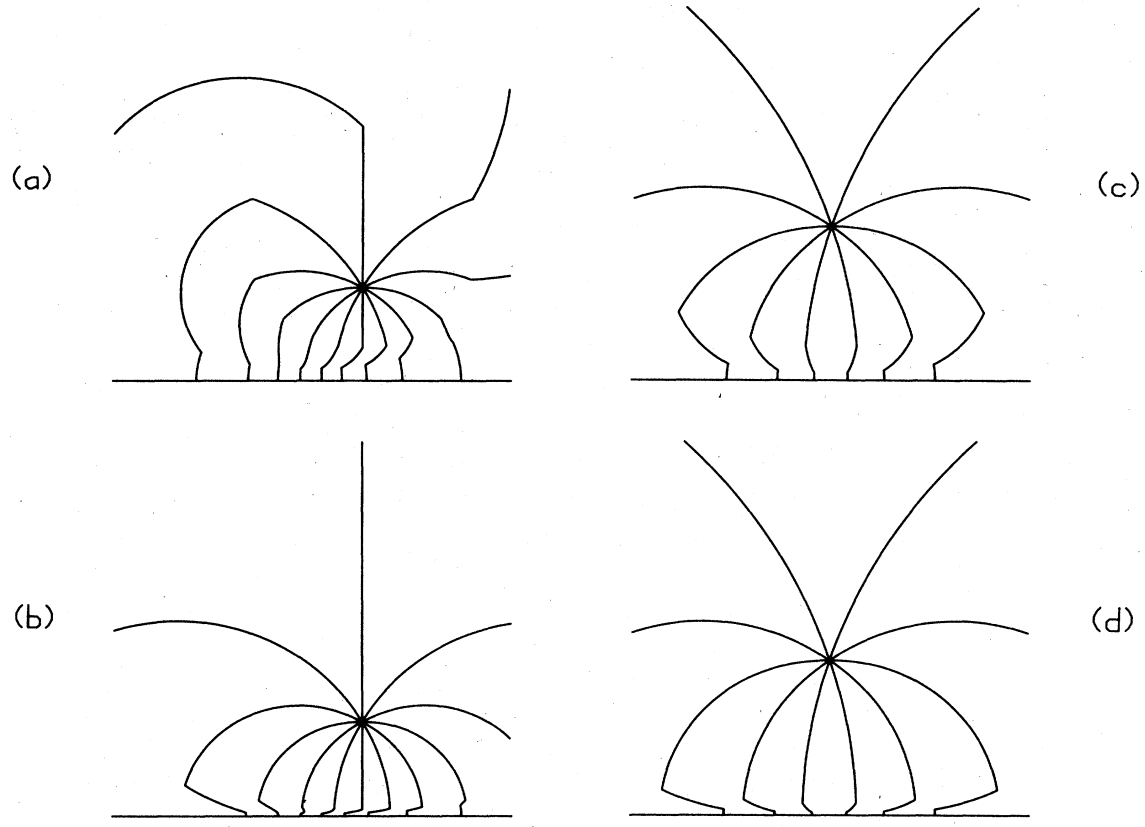

FIG. 8. Electric field lines of temporarily moving charges in the neighborhood of the Rindler horizon. Diagrams (a) and (b) show the field of a charge which moves with constant velocity parallel to the horizon, $d\mathbf{x}/d\tau=\beta\mathbf{e}_x$, from $t=0$ to $t=1/g_H$ and is static before and after this motion. In both diagrams, $\beta=0.5$; diagram (a) shows the field at $t=2/g_H$, and diagram (b) shows it at $t=3.5/g_H$. Diagrams (c) and (d) show the field of a charge which moves with constant velocity perpendicular to the horizon, $d\mathbf{x}/d\tau=\beta\mathbf{e}_z$, from $t=0$ to $t=1/g_H$ and is static before and after this motion. In both diagrams, $\beta=0.5$; diagram (c) shows the field at $t=2.5/g_H$, and diagram (d) shows it at $t=3.5/g_H$.

the $-x$ direction. The current flow produces Joule heating and a Lorentz force in the horizon, which dissipate the energy and momentum carried by the field in the transition region. For times $t\gg 1/g_H$, the field on and above the stretched horizon returns to a fully static configuration (last diagram of Fig. 3).

The qualitative features of the tangential field structure observed in the above problem are not unique to it, but rather they are a general feature of any field lines that move in the vicinity of a horizon.

For example, consider a problem where we move an initially static charge perpendicular to the horizon with constant ZAMO-measured velocity β during the time interval $0<t<1/g_H$. In this interval, the charge has a trajectory $z=z_0e^{g_H\beta t}$ (upward motion) and a four-velocity $u^\alpha=(\gamma/\alpha,0,0,\gamma\beta)$ where $\gamma\equiv(1-\beta^2)^{-1/2}$. Putting this into Eqs. (3.6) and (3.8), we have the electric field:

$$E_\rho=\frac{Q\tilde{\rho}}{z_0^2}\frac{(1-\beta^2)(\tilde{\alpha}e^{-g_H\beta t_R}-\beta S)}{[\tilde{\alpha}(S-\beta C)+\beta e^{g_H\beta t_R}]^3},$$
$$E_z=\frac{Q}{z_0^2}\frac{\tilde{\alpha}(1-\beta^2)(\tilde{\alpha}e^{-g_H\beta t_R}-\beta S-C)}{[\tilde{\alpha}(S-\beta C)+\beta e^{g_H\beta t_R}]^3}, \tag{3.31}$$

where $\tilde{x}\equiv x/z_0$, $\tilde{y}\equiv y/z_0$, $\tilde{\alpha}\equiv z/z_0$, $\tilde{\rho}\equiv[(\tilde{x}^2+\tilde{y}^2)]^{1/2}$, $S\equiv\sinh g_H(t-t_R)$, $C\equiv\cosh g_H(t-t_R)$, and the retarded time t_R is defined implicitly by

$$\tilde{x}^2+\tilde{y}^2+\tilde{\alpha}^2+e^{2g_H\beta t_R}-2\tilde{\alpha}e^{g_H\beta t_R}\cosh g_H(t-t_R)=0\ .$$

Figures 8(c) and 8(d) show the field lines at $t=2.5/g_H$ and $t=3.5/g_H$, respectively. The qualitative features are clearly the same as in the case of the charge moved parallel to the horizon, and again we see a tangential structure traveling down to the stretched horizon. In this case, the current flows radially outward and distributes the induced charge over a larger region in the new static situation.

For further insight into the evolution of the electric field, we show in Fig. 9(a) the evolution of the direction of a particle's electric field as the field "propagates" near the horizon. More specifically, we consider the particle of Figs. 4(a), 5, 6, and 7 which is moving parallel to the horizon (x direction) with a locally measured velocity $\beta=0.5$. The particle's field, as described by the Liénard-Wiechert potential (3.5), propagates away from the particle with the speed of light. (Of course, this is strictly true only close to the horizon where the spacetime curvature and its scattering effects are negligible.) In Fig. 9(a), we study

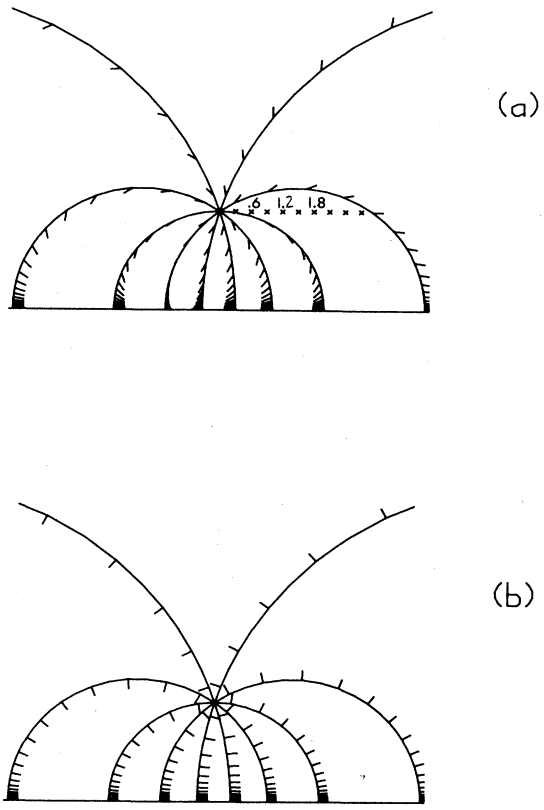

FIG. 9. Constant-time-interval snapshots of the field of a charge moving with $\beta=0.5$ in the x direction, parallel to the horizon [charge of Figs. 4(a), 5, 6, and 7]. The figure shows the directions of those bits of field (indicated by the short segments, or arrows) that were "emitted" by the particle when it was at the point to which the curved lines converge. The curved lines are the spatial tracks of the null geodesics along which the field propagates, and the direction of the field is indicated by the arrows on them. Part (a) shows the electric field in the x-z plane with a snapshot interval $\Delta t=0.3/g_H$. Also shown are the positions of the particle (crosses) at the times of the successive snapshots, labeled by the time t in units of $1/g_H$. Part (b) shows the magnetic field in the y-z plane with a snapshot interval $\Delta t=0.3/g_H$.

the propagation in the x-z plane of that piece of the electric field which is emitted by the particle at time $t=0$, when the particle is at the point from which the curved lines diverge. These curved lines are the spatial tracks of the null geodesics along which that bit of field propagates. Each short segment, or arrow, depicts the direction that the field points when it has reached the location, on its propagation geodesic, where the arrow's tail sits. Thus, the first set of arrows in Fig. 9(a) (those nearest the particle's position) constitute a snapshot of the field at a time $t=0.3/g_H$ after the emission event—when the particle has moved to the location of the first cross. The second set of arrows is a snapshot of the field at $t=0.6/g_H$, when the particle has reached the cross marked 0.6. Each successive snapshot and particle location is at a subsequent time interval $\Delta t=0.3/g_H$. When the fields generated are still in the region close to the charge, they behave essentially in a Minkowskian way, except that those parts that travel upward move faster as α gets larger and those parts traveling downward toward the horizon move more slowly as α get smaller. Recall that in flat-space electrodynamics, the electric field lines of a uniformly moving charge always point toward the present position of the charge. For the case of a particle near the Schwarzschild or Rindler horizon, however, the parts of the field traveling away from the horizon point in front of the present position of the charge, while those parts traveling downward toward the horizon point to the rear of it and eventually become tangential to the horizon.

Had we chosen to take snapshots at constant intervals of $\tilde{t}$ [Eq. (3.30)], the field propagating on the null trajectories would march through the horizon without hesitation; but since we use constant intervals of universal time t, we take an infinite number of snapshots of the field in the region just outside the horizon. Therefore, we see an unchanging field structure as t progresses: the fossil field structure described in Sec. II. The introduction of the stretched horizon simply cuts off the redundant taking of snapshots at a convenient surface outside the horizon.

All of the above figures and conclusions have pertained to the electric field of a moving charge. It is of interest also to investigate the evolution of a magnetic field near a black-hole horizon. From the curved-space Maxwell equations (2.3d), it is seen that, in regions of space with no sources, the duality transformation $\mathbf{E}\rightarrow\mathbf{B}$ and $\mathbf{B}\rightarrow-\mathbf{E}$ preserves the form of the equations and hence their solutions, just as in flat-space electrodynamics. Therefore all of the qualitative conclusions reached above for an electric field will hold also for a magnetic field.

More specifically, for a static magnetic field, as for a static electric field, the field lines will intersect the stretched horizon orthogonally, so that by Eq. (2.6b) there is no surface current to produce dissipation. If the magnetic field is disturbed, the disturbance will propagate down toward the horizon and form a tangential structure. This assertion is supported by Fig. 9(b), which shows the magnetic field generated by the uniformly moving particle of Fig. 9(a) propagated along null trajectories in the y-z plane, in the same manner as was done for the electric field in Fig. 9(a). Note here, as for the electric field, that the field structure becomes tangential near the horizon. When this structure sinks through the stretched horizon, a current is induced which dissipates the Maxwell field energy and momentum. The effect of this process is to "clean" the magnetic field by removing complicated tangential structure near the horizon. This process might be important in models of quasars which involve large magnetic fields in the neighborhoods of black-hole horizons.[15] A model problem relevant to this process will be considered in the next section.

IV. RELAXATION OF A MAGNETIC FIELD IN SCHWARZSCHILD SPACETIME

The preceding section considered electromagnetic model problems in Schwarzschild spacetime in a region

close enough to the horizon that the Rindler approximation could be adopted. If the Rindler approximation is dropped, the mathematics of these problems generally becomes more difficult. The spatial curvature which was ignored in the transition from Schwarzschild to Rindler makes the three-space vector operators, and thus Maxwell's equations, considerably more complicated in the full Schwarzschild spacetime. However, it is instructive to investigate a model problem in the full Schwarzschild black-hole background to verify that the models we have made using the Rindler approximation have not omitted any important features of the interaction of electric and magnetic fields with a horizon and also to develop intuition concerning the effect of spatial curvature on those fields.

We consider the problem of a Schwarzschild black hole of mass M, surrounded by a perfectly conducting concentric sphere of radius $R > 2M$ into which an axially symmetric magnetic field is frozen. At time $t=0$, the magnetic field lines are momentarily static and purely radial, pointing into the hole below the equator and out of the hole above it, as shown in the upper left-hand diagram in Fig. 10. Immediately after time $t=0$, this initial configuration is released and allowed to evolve dynamically in accord with the vacuum Maxwell equations, except that the field lines continue to be held fixed in the conducting sphere at radius R. We shall study the dynamical evolution of this field.

In Schwarzschild coordinates (t,r,θ,ϕ), where the lapse function is $\alpha=\sqrt{1-2M/r}$, the initial electric and magnetic fields are

$$\mathbf{E}=0\ ,$$
$$\mathbf{B}=B_0\alpha\left[\frac{R}{r}\right]^2\cos\theta\frac{\partial}{\partial r}=B_0\left[\frac{R}{r}\right]^2\cos\theta\mathbf{e}_{\hat{r}}\ , \tag{4.1}$$

and the corresponding initial vector potential is purely toroidal:

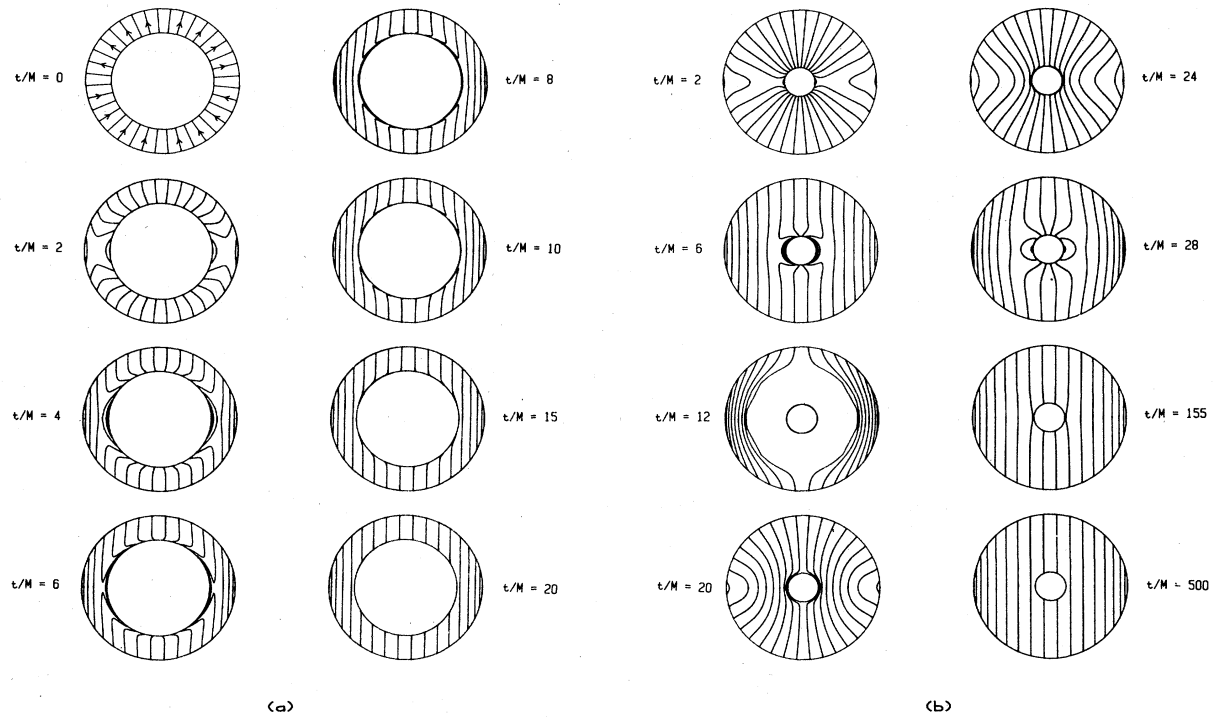

FIG. 10. The vibratory time evolution of an initially radial magnetic field in Schwarzschild spacetime. The initial geometry of the magnetic field lines is shown in the upper left-hand diagram of part (a) in r-θ coordinates with $\phi=$constant. The outer boundary, at which a perfectly conducting sphere resides, is at radius $r=R$; the inner sphere is the horizon. The arrows show the direction of the field: pointing into the hole below the equator and out of the hole above it. This is the view which would be seen by looking down into the paraboloidal embedding diagram of Schwarzschild space. The field lines are frozen into the outer sphere, but are free to slip through the horizon since its conductivity is finite. The tension of the field lines tends to straighten them out. Part (a) shows representative magnetic-field-line diagrams in the evolution of the case $R=3M$. Since most of the field lines thread the horizon at all times, the field settles down quickly to its final static configuration. Part (b) shows representative magnetic-field-line diagrams in the evolution of the case $R=10M$. Since the horizon is small relative to the outer sphere, the field lines oscillate for a long time before reaching their final static configuration. The diagrams in part (b) cover only the first oscillation in detail, and the beginning of the second oscillation at $t/M=28$. The last two diagrams are much further in the future and show that the oscillations have died out substantially by $t/M=155$ and almost completely by $t/M=500$. The kinks in the field lines for the case $t/M=12$ are due to the finite grid used in the numerical integration.

$$\mathbf{A}=\frac{B_0R^2}{2r}\sin\theta\mathbf{e}_{\hat{\phi}}\ , \tag{4.2}$$

where B_0 is the magnetic field strength on axis at the outer sphere and $\mathbf{e}_{\hat{\phi}}\equiv(1/r\sin\theta)\partial/\partial\phi$. [Throughout this section, carets will be used to denote the orthonormal basis $(\mathbf{e}_{\hat{r}},\mathbf{e}_{\hat{\theta}},\mathbf{e}_{\hat{\phi}})$.]

The field lines are fixed at their outer ends because they are frozen into the perfectly conducting outer sphere, but they are free to slip through the stretched horizon since it has a finite conductivity. Qualitatively, one would expect the field lines to pull themselves into a more vertical orientation due to their tension.

The symmetries of the problem, along with Maxwell's equations, ensure that all components of the four-vector potential except $A_\phi(t,r,\theta)$ will remain zero. This component may be written in terms of the "magnetic flux function" $\psi(t,r,\theta)\equiv 2\pi A_\phi(t,r,\theta)$ which, as shown in MT, is equal to the total magnetic flux through the circle of constant radius and latitude $(r,\theta)=$constant. The expressions for the electric and magnetic fields in terms of ψ are

$$\mathbf{E}=-\frac{1}{\alpha}\dot{\mathbf{A}}=-\frac{\dot{\psi}\mathbf{e}_{\hat{\phi}}}{2\pi\alpha r\sin\theta}\ ,$$
$$\mathbf{B}=\nabla\times\mathbf{A}=\frac{\nabla\psi\times\mathbf{e}_{\hat{\phi}}}{2\pi r\sin\theta}\ , \tag{4.3}$$

where the overhead dot denotes time differentiation. The only nonvacuous Maxwell equation is Ampere's law [MT Eq. (2.17c)], which, specialized to vacuum Schwarzschild spacetime and expressed in terms of ψ, may be written as

$$\nabla\cdot\left[\frac{\alpha}{r^2\sin^2\theta}\nabla\psi\right]-\frac{1}{\alpha r^2\sin^2\theta}\ddot{\psi}=0\ . \tag{4.4}$$

The covariant three-space derivatives in the vector operators in this equation may be expanded in terms of ordinary derivatives, with the result

$$-\frac{\psi_{,tt}}{1-2M/r}+\left[1-\frac{2M}{r}\right]\psi_{,rr}+\frac{2M}{r^2}\psi_{,r}+\frac{\psi_{,\theta\theta}}{r^2}-\frac{\cot\theta}{r^2}\psi_{,\theta}=0\ . \tag{4.5}$$

By introducing the "tortoise coordinate" r^* of Regge and Wheeler[31] defined by

$$dr^*=\frac{dr}{1-2M/r}\ ,$$
$$r^*=r+2M\ln\left[\frac{r}{2M}-1\right]\ , \tag{4.6}$$

Eq. (4.5) can be put into the form

$$-\psi_{,tt}+\psi_{,r^*r^*}+\frac{1}{r^2}\left[1-\frac{2M}{r}\right](\psi_{,\theta\theta}-\cot\theta\psi_{,\theta})=0\ . \tag{4.7}$$

In this equation, r is to be thought of as an implicitly defined function of r^*.

The boundary condition of "no outgoing waves at the horizon" [Eq. (2.9)] requires

$$[\mathbf{E}_{||}-\mathbf{n}\times\mathbf{B}_{||}]_{r\to 2M}\to 0\ , \tag{4.8}$$

where $\mathbf{n}$ is the unit normal vector $\mathbf{e}_{\hat{r}}$ to the horizon and $\mathbf{E}_{||}$ and $\mathbf{B}_{||}$ are the field components tangential to the horizon. The tangential fields may be expressed in terms of the potential ψ as

$$\mathbf{E}_{||}=-\frac{1}{2\pi\alpha r\sin\theta}\frac{\partial\psi}{\partial t}\mathbf{e}_{\hat{\phi}}\ ,$$
$$\mathbf{B}_{||}=\frac{[\nabla\psi\times\mathbf{e}_{\hat{\phi}}]_{||}}{2\pi r\sin\theta}=-\frac{\alpha}{2\pi r\sin\theta}\frac{\partial\psi}{\partial r}\mathbf{e}_{\hat{\theta}}\ , \tag{4.9}$$

so the horizon boundary condition (4.8) becomes

$$\left[\frac{\partial\psi}{\partial t}-\frac{\partial\psi}{\partial r^*}\right]_{r\to 2M}\to 0\ . \tag{4.10}$$

The initial field

$$\mathbf{A}=(2\pi r\sin\theta)^{-1}\psi(0,r,\theta)\mathbf{e}_{\hat{\phi}}=B_0(R^2/2r)\sin\theta\mathbf{e}_{\hat{\phi}}$$

has the angular dependence of the $l=1$, $m=0$ vector spherical harmonic[27] $\mathbf{X}_{1,0}(\theta,\phi)=i\sqrt{3/8\pi}\sin\theta\mathbf{e}_{\hat{\phi}}$; and since neither the differential equation (4.7) nor the boundary conditions mix different multipoles, the field will remain proportional to this harmonic as it evolves. It is thus convenient to separate variables by defining a new field variable $u(t,r)$:

$$\psi(t,r,\theta)=\pi B_0R^2u(t,r)\sin^2\theta\ . \tag{4.11}$$

Then the wave equation (4.7) for ψ takes the form

$$-u_{,tt}+u_{,r^*r^*}-\frac{2}{r^2}\left[1-\frac{2M}{r}\right]u=0\ . \tag{4.12}$$

This equation describes a one-dimensional wave subject to a potential $V(r^*)\equiv 2(1-2M/r)/r^2$. This potential goes to zero at the horizon proportionally to $\alpha^2\simeq e^{2g_Hr^*}$, goes to zero as $r^{-2}\simeq(r^*)^{-2}$ at large r, and has a global maximum at $r=3M$ ($r^*\simeq 1.61M$), $V_{\max}=2/(27M^2)$. The inner boundary condition (4.10) written in terms of $u(t,r)$ is just

$$\left[\frac{\partial u}{\partial t}-\frac{\partial u}{\partial r^*}\right]_{r\to 2M}\to 0\ , \tag{4.13}$$

which has the form of a "perfectly absorbing" boundary condition for the one-dimensional wave equation (4.12). The outer boundary condition is $u(t,R)=1$, and the initial conditions are $u(0,r)=1$ and $u_{,t}(0,r)=0$.

The wave equation (4.12) was integrated numerically subject to these initial and boundary conditions, and the structure of the magnetic field lines was then reconstructed from $u(t,r)$ using the relation (4.11) and the definition of $\psi(t,r,\theta)$ as the magnetic flux function [Eq. (4.9)]. The inner boundary condition (4.13) was applied not at the actual horizon $r^*=-\infty$, but at a slightly stretched horizon $r^*=-20M$, which corresponds to the Schwarzschild radius $r=(2+3.3\times10^{-5})M$ and $\alpha_H=4.1\times10^{-3}$. (Although this horizon stretching is motivated by numerical considerations, it is the same stretching as occurs in the membrane viewpoint.) Representative plots of the mag-

netic field line structure are shown in Figs. 10(a) and 10(b) for the cases $R=3M$ and $R=10M$, respectively.

The qualitative behavior of the solutions, as depicted in r-θ coordinates, is that the field oscillates for a time before settling down to a final static configuration consisting of precisely vertical field lines. The final static configuration could be derived directly by setting the time derivatives in Eq. (4.12) to zero, and solving it subject to the boundary conditions $u(r=R)=1$ and $u_{r^*}(r=2M)=0$; it is the solution $\psi(r,\theta)=\pi B_0 r^2\sin^2\theta$ found by Wald[32] and by Hanni and Ruffini.[33]

As the field lines oscillate, they leave behind disconnected field-line loops near the horizon, such as those shown in the diagram for $t/M=28$ in Fig. 10(b). These loops drop toward the horizon at the locally measured speed of light, $dr^*/dt\sim 1$ or $dr/dt\sim\alpha^2$. Thus, as described qualitatively in Sec. II, the field has a layered structure at the horizon which reflects the entire past history of its evolution. However, these layered horizon fields do not affect the overall large-scale structure of the field outside the horizon; the position of the stretched horizon in the numerical integration could be moved outward considerably without changing the diagrams in Fig. 10 in any noticeable way.

The complex, multilayered nature of the near-horizon fields is illustrated graphically in Fig. 11. In the top part of this figure, the magnetic field lines are plotted on an embedding diagram for Schwarzschild spacetime, which consists of a paraboloid of revolution.[11] In this part of the diagram, the Schwarzschild radial coordinate r is measured radially outward from the axis of cylindrical symmetry of the embedding diagram, and the angular coordinate θ is measured around this axis. The ignorable coordinates t and ϕ are suppressed. The diagrams in Fig. 10 are what one would see if one were looking down into the paraboloid along the axis of symmetry. The paraboloid of the embedding diagram is cut off at a stretched horizon which is taken to be at a radius $r=2.15M$. [As will be explained later, this would be a poor choice of stretched horizon at which to apply the boundary condition (4.13), but it is chosen here for illustrative purposes.] In order to make the fields between the stretched horizon and the true horizon visible, they are plotted on a cylinder matched to the paraboloid at the stretched horizon. In this part of the diagram, the vertical distance, i.e., the cylindrical "z coordinate," is equal to the tortoise coordinate r^*, and the previous identification of θ with the cylindrical angular coordinate is maintained. Plotting the near-horizon fields in this way as functions of r^* has the effect of expanding the radial scale so that the field structure is visible.

The data plotted in Fig. 11 show the field-line structure at the time $t=92M$ for the case $R=10M$. At this time, the field lines have sprung outward and snapped back inward four times and are beginning to spring outward for a fifth time. The relic field-line loops left by each of these oscillations are visible running down the cylinder, and the partially formed loops at the top of the cylinder may be seen to connect to field lines outside the stretched horizon. The field lines are vertical in the lowermost region of the diagram due to the fact that the field was held stationary until its release at $t=0$. As one proceeds up the cylinder, one finds successively fewer concentric loops in each set of field lines since the oscillations are dying out and fewer field lines snap back to the stretched horizon with each oscillation.

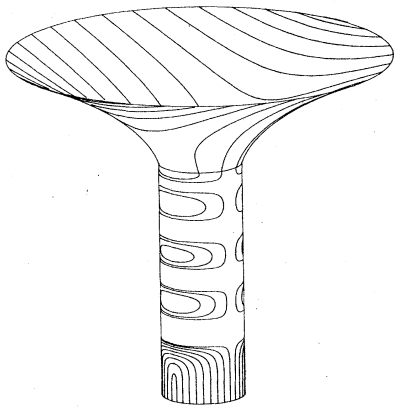

FIG. 11. Embedding-diagram view of the vibrating magnetic field of Fig. 10 at time $t=92M$ for the case $R=10M$, with the near-horizon fields expanded for visibility. In the top part of the figure, the magnetic field lines are plotted on the paraboloidal embedding diagram of Schwarzschild space. The paraboloid is cut off at a stretched horizon which is taken to be at a radius $r=2.15M$, and a cylinder is matched onto it there. In order to make the near-horizon fields visible, the distance along this cylinder is measured by the tortoise coordinate r^*. We view the diagram from an elevation angle of 18° and a rotation angle of 45°. At the time shown, the field lines have sprung outward and snapped back inward four times and are beginning to spring outward for a fifth time. The relic field-line loops left by each of these oscillations are visible running down the cylinder, and the partially formed loops at the top of the cylinder may be seen to connect to field lines outside the stretched horizon. In the lowermost region of the diagram, the field lines are vertical due to the fact that the field was held stationary until its release at $t=0$. As one proceeds up the cylinder, one finds successively fewer concentric loops in each set of field lines, since the oscillations are dying out and fewer field lines snap back to the stretched horizon with each oscillation.

Two criteria need to be considered in choosing the position of the stretched horizon in a problem of this sort. The potential $V(r^*)$ in Eq. (4.12) acts as a barrier to incoming waves, partially transmitting them and partially reflecting them. Application of the "perfectly absorbing" boundary condition at the stretched horizon rather than at the true horizon is equivalent to neglecting waves reflected from the part of the potential barrier (spacetime curvature) between the two horizons. Since $V(r^*)$ goes to zero proportionally to α^2 near the true horizon, this approximation becomes better and better as the stretched horizon is moved inward toward the true horizon. In the problem at hand, it was found that moving the stretched horizon from its original location $r^*=-20M$ out to $r^*=-10M$ or $r=(2+4.9\times 10^{-3})M$ made no noticeable difference in the numerical solutions obtained. On the other hand, putting the stretched horizon at $r=2.15M$, as was done in

Fig. 11 for illustrative purposes, should not be done in the numerical solution of the problem since $V(r^*)$ still has 41% of its maximum value there.

The other criterion affecting the choice of the stretched horizon is the requirement that it be close enough to the true horizon that important features of the field are not neglected below the stretched horizon. More specifically, we demand that α_H be small enough that the field does not evolve substantially along any null ray between $\alpha=\alpha_H$ and $\alpha=0$. In terms of the Eddington-Finkelstein time coordinate $\tilde{t}$ of Eq. (2.4), the equation of such a null ray is $dr/d\tilde{t}=-1$. If Δt is the (universal) timescale of evolution of the field, the above criterion translates into the requirement that $\alpha_H \lesssim \sqrt{2g_H \Delta t}$. This condition is certainly satisfied in the present problem for either of the choices of the stretched horizon mentioned above, since the timescale of variation of the field is $\Delta t \sim M$.

The only dissipation in this problem comes from the horizon boundary condition. If the stretched horizon had a surface resistivity of either zero or infinity, rather than presenting incoming waves with the vacuum impedance $R_H=4\pi\simeq 377\ \Omega$, the field lines would oscillate forever. The damping timescale of the oscillations is determined by the size of the horizon relative to the perfectly conducting outer sphere: for the case $R=3M$, the field lines almost settle down to the static configuration after springing outward just once, while for the case $R=10M$, they oscillate many times.

The magnetohydrodynamical decay time of a field slipping through a conducting medium with surface resistivity R_H may be shown[34] to be roughly equal to $4\pi L/R_H$, where L is a length comparable with the dimensions of the region where current flows. For the present problem, where $L\sim 2M$, this timescale is just $2M$, the light-travel time across the hole (which, as claimed in Sec. 7.5 of MT, is the approximate annihilation time for a field loop with both feet in the hole). Not all of the field lines are dissipating their vibrational energy in the hole at a particular time, however. One would therefore expect the timescale t_* of the relaxation of the field lines to be roughly equal to $2M$ divided by the time-averaged fraction of field lines which thread the horizon, which is approximately $4M^2/R^2$; that is

$$t_* \sim 2M\left[\frac{R^2}{4M^2}\right]=\frac{R^2}{2M}\ . \tag{4.14}$$

The time t_* is the timescale of the loss of magnetic field energy into the hole, so it will be instructive to elaborate further on the nature of the transfer of electromagnetic energy into the hole.

Following MT, one may define a density ϵ_E and flux density $\mathbf{S}_E$ of "red-shifted energy" or "energy at infinity":

$$\epsilon_E \equiv (\alpha/8\pi)(\mathbf{E}^2+\mathbf{B}^2)=\frac{\alpha}{32\pi^3 r^2\sin^2\theta}\left[\frac{\dot{\psi}^2}{\alpha^2}+(\nabla\psi)^2\right]\ , \tag{4.15a}$$

$$\mathbf{S}_E \equiv (\alpha/4\pi)\mathbf{E}\times\mathbf{B}=-\frac{\dot{\psi}\nabla\psi}{16\pi^3 r^2\sin^2\theta}\ . \tag{4.15b}$$

These satisfy the conservation law

$$\frac{d}{dt}\int_V \epsilon_E dV+\int_{\partial V}\alpha\mathbf{S}_E\cdot d\mathbf{A}=0\ , \tag{4.16}$$

for any time-independent three-dimensional region V lying entirely exterior to the horizon and having the two-dimensional boundary surface ∂V. Here $d\mathbf{A}$ is the outward-pointing normal area element vector.

One may also write the charge and current densities on the stretched horizon as defined in Sec. II. If we take the stretched horizon to be at r_H, the charge density vanishes and the current density (2.6b) is

$$\mathcal{J}_H=\frac{1}{4\pi}\mathbf{e}_{\hat{r}}\times\mathbf{B}_H=-\frac{1}{8\pi^2 r_H\sin\theta}\frac{\partial\psi}{\partial r^*}\mathbf{e}_{\hat{\phi}}\ , \tag{4.17}$$

where $\mathbf{B}_H$, the stretched-horizon magnetic field, is defined by Eq. (2.5). The stretched-horizon current density is thus purely toroidal, and from Eq. (4.11) one may see that it varies with latitude proportionally to $\sin\theta$.

If we take the region V in Eq. (4.16) to be the spherical shell between the stretched horizon and the outer radius $r=R$, then the only contribution to the surface integral in Eq. (4.16) comes from the stretched horizon, since there is no energy flux through the perfectly conducting sphere at $r=R$. The rate of mass increase of the hole per unit universal time is equal ("$\cong$", in the sense of Sec. II) to the rate of energy flow, per unit universal time t, through the stretched horizon. Using Eqs. (4.6), (4.9), (4.15b), and (4.17), this may be expressed as

$$\frac{dM}{dt}\cong\int_{\mathrm{SH}}\alpha\mathbf{S}_E\cdot d\mathbf{A}=\int_{\mathrm{SH}}\mathcal{J}_H\cdot\mathbf{E}_H dA\ , \tag{4.18}$$

in agreement with Eq. (2.11). Here the area element vector $d\mathbf{A}$ points along the outward normal to the region V and hence along the *inward* normal to the horizon. By integrating Eq. (4.16) over time, one may obtain the difference between the total energies of the field in the initial (E_i) and final (E_f) configurations:

$$E_f-E_i=\Delta\int_V\epsilon_E dV=-\int_0^\infty\left[\int_{\mathrm{SH}}\mathcal{J}_H\cdot\mathbf{E}_H dA\right]dt \cong -(M_f-M_i)\ , \tag{4.19}$$

where M_i and M_f are the initial and final masses, respectively, of the hole.

The quantities E_i and E_f may be obtained explicitly by integrating the energy density ϵ_E over the region V using the initial and final fields: $\psi_i=\pi B_0 R^2\sin^2\theta$ and $\psi_f=\pi B_0 r^2\sin^2\theta$, respectively. The results are

$$E_i\cong\frac{B_0^2R^4}{12M}\left[1-\frac{2M}{R}\right]\ ,\qquad E_f\cong\frac{B_0^2R^3}{6}\left[1-\frac{2M}{R}\right]\ . \tag{4.20}$$

The rate of energy flow through the stretched horizon can be calculated from Eqs. (4.11), (4.13), (4.17), and (4.18) to be

$$\frac{dM}{dt} \cong \int_{\mathrm{SH}} \mathcal{S}_H \cdot \mathbf{E}_H dA \cong \frac{B_0^2 R^4}{6} \left[\frac{\partial u}{\partial r^*} \right]_{\mathrm{SH}}^2 . \tag{4.21}$$

The quantity $(\partial u/\partial r^*)^2_{\mathrm{SH}}$, which by Eq. (4.21) is proportional to the energy flux through the stretched horizon, is plotted in Fig. 12 for the cases $R=3M$, $R=10M$, and $R=100M$. The displacement of the first peak from the origin in these diagrams is due to the finite time required for the waves to propagate down to the stretched horizon. It has been verified numerically that the area under these curves satisfies the energy balance condition, Eq. (4.19), i.e.,

$$\begin{aligned} E_f - E_i &= -\frac{B_0^2 R^4}{6} \int_0^\infty \left[\frac{\partial u}{\partial r^*} \right]_{\mathrm{SH}}^2 dt \\ &\cong -\frac{B_0^2 R^4}{12M} \left[1 - \frac{2M}{R} \right]^2 \\ &\Longleftrightarrow \int_0^\infty \left[\frac{\partial u}{\partial r^*} \right]_{\mathrm{SH}}^2 dt \cong \frac{(1-2M/R)^2}{2M} . \end{aligned} \tag{4.22}$$

The curve for $R=100M$ in Fig. 12 seems to be a superposition of two oscillations of distinct periods, a fact which may be confirmed by Fourier transforming it. The period of the longer-term oscillation is approximately twice the radius R of the outer shell, i.e., roughly the light-travel time across the shell. This just corresponds to the time necessary for a particular field line to spring outward and then back inward.

The period of the shorter-term oscillation is roughly equal to $10M$. This value may be justified by an argument similar to that used by Press[35] for gravitational waves. An argument precisely analogous to that given by Press predicts that $u(t,r)$ should have a peak in its frequency spectrum corresponding to a period

$$T \sim \frac{2\pi}{V_{\max}^{1/2}} = 3\pi\sqrt{6}M \sim 23M . \tag{4.23}$$

Since the energy flux curves in Fig. 12 are proportional to the squares of $\partial u/\partial r^*$, they should have roughly half this period, or about $10M$ as observed. This argument could also be couched in terms of the gradual decay of a packet of electromagnetic waves in spiral orbits close to the unstable photon orbit at $r=3M$, as Goebel[36] does for gravitational waves.

Thus, the short period might be characterized as the "sticking time," during which the oscillating field lines are caught and held by the effective potential, while the long period is the natural vibration time of the field lines.

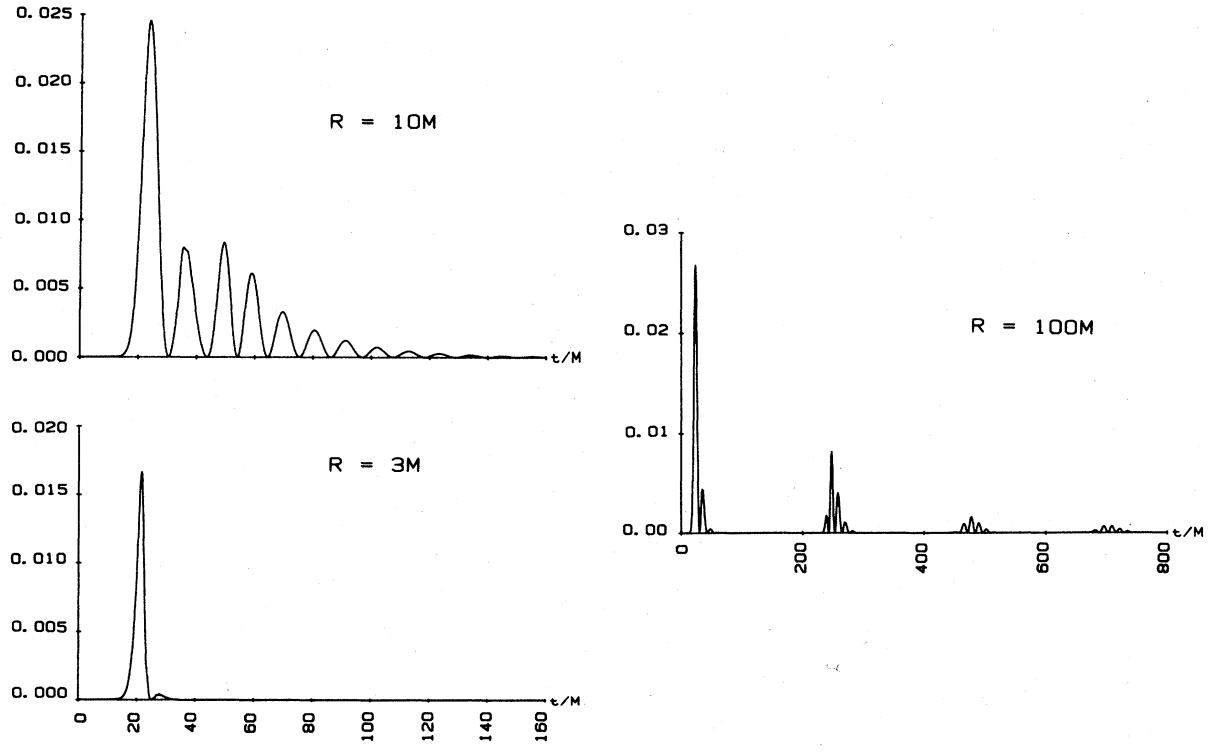

FIG. 12. The rate of flow of magnetic energy through the horizon as a function of time for the vibrating magnetic field of Figs. 10 and 11. Plots are shown for three different values of the radius of the outer conducting sphere: $R=3M$, $R=10M$, and $R=100M$. Plotted vertically is the dimensionless quantity $M^2(\partial u/\partial r^*)^2_{\mathrm{SH}}$ which, as shown in Eq. (4.21), is proportional to the energy flux through the horizon. The curve for $R=100M$ shows a clear double periodicity corresponding to the two different length scales in the problem: R and M.

The double periodicity noticeable in the $R=100M$ curve of Fig. 12 is not evident in the $R=3M$ and $R=10M$ cases since the two periods are too close together in the $R=10M$ case and the oscillations die out too soon in the $R=3M$ case.

This double periodicity somewhat complicates the task of finding an "experimental" relationship between the damping timescale t_* and the cavity radius R to compare with the "theoretical" relationship (4.14). The curves consist of periods of oscillation interspersed with periods of quiescence, so a good fit to an exponential decay is impossible. However, rough fits to the envelopes of the curves yield decay times which conform approximately to a power law relationship of the form $t_*/M=\beta(R/M)^\gamma$. The values of γ given by a least squares log-log fit ranged from 1.6 to 1.8 depending on the assumptions made in the fits to the envelopes, and the values obtained for β ranged from 0.4 to 0.6. The theoretical relationship (4.14) would predict the values $\beta=0.5$ and $\gamma=2$.

The results of this model problem and those considered in Sec. III suggest some very general conclusions concerning the nature of a stationary electromagnetic field outside

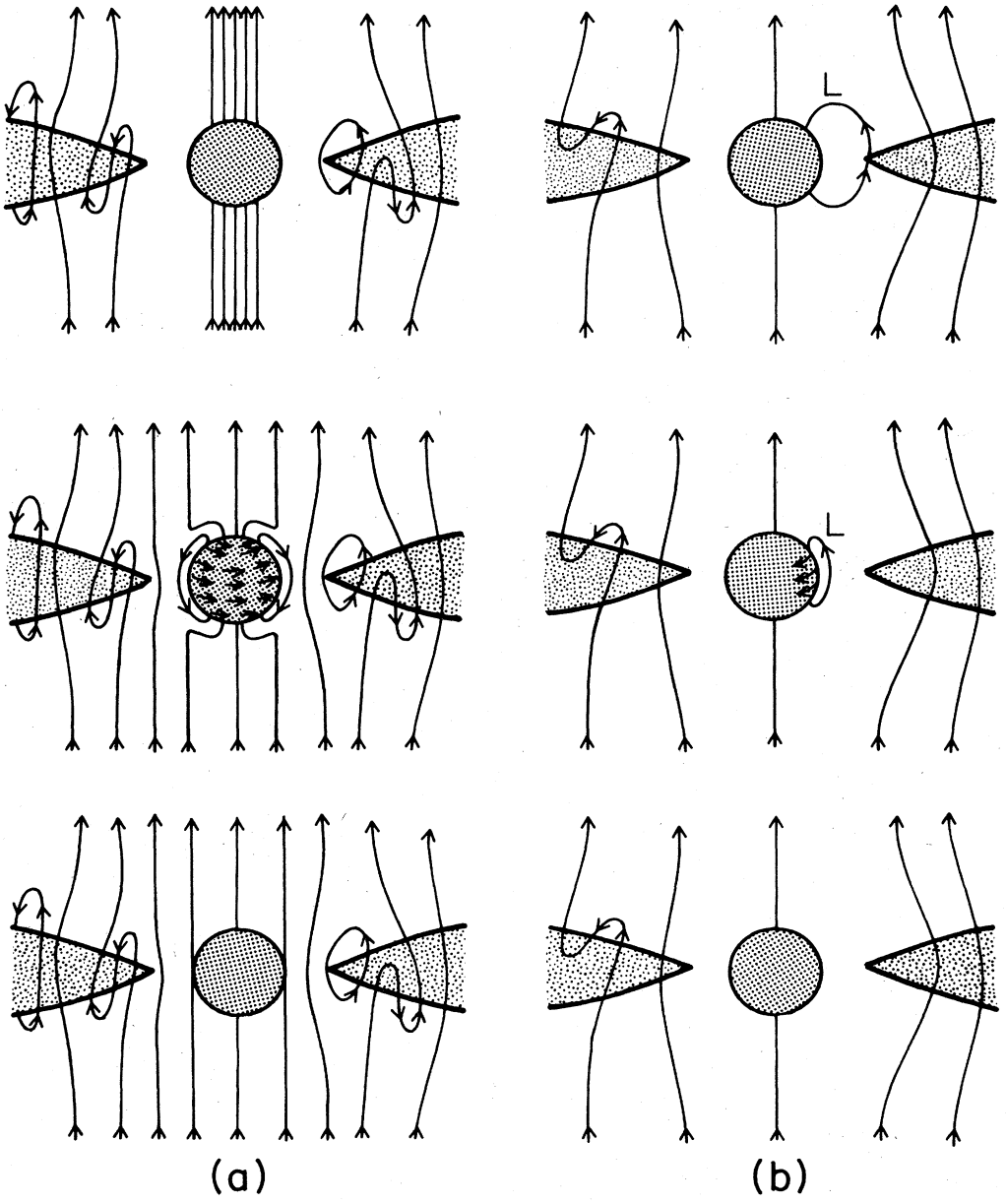

FIG. 13. Qualitative illustrations of the "cleaning" of a complex electromagnetic field by a black-hole horizon. Part (a) shows the dispersal of a localized concentration of magnetic flux threading the horizon. Part (b) shows the annihilation of a field-line loop, marked "L," with both feet embedded in the horizon. In both cases, the horizon currents, which dissipate excess field energy, are indicated by arrows on the horizon.

a black hole. In paper II of this series (MT Sec. 7.5), an analysis of the equations of structure for a stationary, force-free black-hole magnetosphere showed that no magnetic field loops can extend out of the horizon and then back in. King, Lasota, and Kundt[37] showed that a stationary magnetic field in a vacuum cavity between a black hole and a surrounding plasma shell must be "nearly uniform," i.e., similar to the final configuration of the field in this section. These results all suggest that, in stationary situations, regardless of the complexity of the electromagnetic fields produced by external (accretion disk) currents in the vicinity of a black hole, the field which actually threads the horizon will be "clean;" it will have no loops or complicated tangential structure near the horizon, and no localized concentrations of magnetic field will exist on any region of the horizon.

Insight gained from the above model problems suggests the mechanism by which a black hole gets rid of such structures (i.e., cleans its field) if they try to form. Figure 13 shows two examples based on the scenario of a magnetic field threading a black hole and held on it by an accretion disk.[15] The material of the disk is slowly spiraling into the hole and dragging its imbedded field, which may be chaotic, onto the hole. In Fig. 13(a) (top), a localized concentration of magnetic flux has formed at a particular point on the horizon. As was observed in the model problem of this section, the field lines will spring outward, driving toroidal currents (shown by arrows on the middle diagram) in the stretched horizon which dissipate the electromagnetic field energy. The field lines may oscillate several times, but within a timescale of order M, the complex, dynamical tangential field will disappear beneath the stretched horizon, leaving just the uniform field shown in the bottom illustration. In Fig 13(b) (top), a loop of magnetic field (labeled "L") has been carried onto the horizon. Tension along the field lines will cause the loop to shorten, bringing itself close to and parallel to the stretched horizon (middle diagram). The loop will then sink into the stretched horizon, driving currents as shown in the middle diagram to dissipate its field energy, until it is completely gone (bottom).

V. DISCUSSION AND CONCLUSION

One of the main strengths of the membrane view of black-hole horizons is the cogent and self-consistent mental picture it provides of the interactions of a horizon with an electromagnetic field. As demonstrated by the model problems in this paper, the membrane viewpoint often allows the qualitative results of calculations to be guessed before they are done. It is important to emphasize, though, that the membrane viewpoint is completely consistent with other viewpoints of black holes, the "black-hole viewpoint" based on Penrose and Eddington-Finkelstein spacetime diagrams, for example. But the membrane viewpoint emphasizes those phenomena which are important in the electromagnetic interaction of a horizon with the exterior universe, and deemphasizes those phenomena, such as the relic tangential horizon field, which are not.

Since the membrane viewpoint is based on a $3 + 1$ split of spacetime, it is particularly well suited to calculations in static or stationary spacetimes. If the spacetime is highly dynamical, however, it loses much of its power since there is then no preferred family of spacelike hypersurfaces with respect to which to make the $3 + 1$ split. In this case, it is more efficacious to view physics in terms of the spacetime diagrams of the black-hole viewpoint. The class of problems for which the membrane formalism is most useful, however, includes most problems of real astrophysical interest. Astrophysical models involving black holes usually assume a nearly stationary and axisymmetric hole interacting electromagnetically, gravitationally, and materially with a complex astrophysical environment (accretion disks, magnetized plasmas, stellar companions, etc.), and for these types of situations the membrane viewpoint is ideally suited. See Ref. 18 for a fuller comparison of the membrane viewpoint with other viewpoints.

In Sec. III, we studied the interaction of external electromagnetic fields with a Schwarzschild horizon in the Rindler approximation. In Sec. IV, a dynamical magnetic field problem in the full Schwarzschild geometry was solved and studied in detail. In both cases, we have illustrated the evolution of the electric and magnetic fields with field-line diagrams. It is the $3 + 1$ formulation in terms of which the membrane formulation is couched which enables such field-line diagrams to be drawn, and this feature contributes greatly to an intuitive understanding of the fields. It was also emphasized in both problems that the concepts of the stretched horizon and its surface charge and current were very helpful in understanding how the presence of the black-hole horizon affects the electromagnetic fields in its vicinity, and in understanding the entropy, energy, and momentum transfer between the field and the hole. In the model problem done in Sec. IV, the criteria governing the choice of the stretched horizon were elucidated: the desire to ignore the relic, near-horizon tangential electromagnetic field, the necessity of making reflection from the electromagnetic potential barrier negligible, and the requirement that the evolution of the field during its propagation from the stretched horizon to the true horizon be negligible. These criteria, although they were derived from consideration of a very specific problem, do not depend on the precise details of that model. This of course is to be desired if the concept of the stretched horizon is to have applicability beyond this limited problem.

The stretched-horizon charges and currents, even though they are entirely imaginary, enter as source terms into Maxwell's equations in exactly the same way as do ordinary charges and currents (although, in the model problems of Secs. III and IV, they turned out to give no contribution to the external field since the black holes under consideration were uncharged). We have seen from the model problems that these concepts facilitate an intuitive understanding of the interactions of a black-hole horizon with external electromagnetic fields. By use of the membrane formalism, both the distortion of an electromagnetic field by the presence of a horizon and the field's effect on the dynamics of the black hole can be understood in close analogy with flat-space electrodynamics.

To elucidate these points more explicitly, we will briefly discuss several black-hole electromagnetic problems in terms of the surface charges and currents. (For further detail on these problems see Ref. 18.) First, we consider the question of how the electric field of a charge very close to, and stationary outside, the Schwarzschild horizon will be distorted by the gravitational field of the hole. This problem was considered in mathematical detail in Sec. III C, but here we are interested in the qualitative features of the solution which can be derived intuitively. Immediately we see that, since the stretched horizon behaves like a conductor, the horizon will be polarized so that charges of the opposite sign are induced in the region under the charge, and the electric field lines will bend to strike the stretched horizon normally.

It is as an aid to intuition rather than as an explicit calculational tool that the membrane viewpoint may find its greatest utility. Although this paper has done no calculations in Kerr spacetime, it is possible to guess the qualitative features of some results which have been derived in the past:

Consider a Kerr hole immersed in a uniform magnetic field aligned with its spin axis. It is natural to regard the stretched horizon of a Kerr black hole as behaving essentially like a rotating conducting surface. A spinning conducting sphere in a magnetic field will develop a charge separation, positive at the equator and negative at the poles, which by Eq. (2.6a) tells us that there will be a normal electric field coming out of the equatorial region and going into the polar regions. Hence we see that the rotation of the Kerr hole couples with the magnetic field to produce a quadrupolar electric field structure. This is verified by the field explicitly calculated by Wald[32], and the analogy is discussed further by Phinney[38] and in Ref. 18.

As another example, one which enables us to examine the effect of an electromagnetic field on the dynamics of a black hole, we consider a Kerr hole immersed in a magnetic field inclined obliquely to its spin axis. For a rotating conducting sphere in an oblique magnetic field, we know that the electromagnetic torque on eddy currents in the sphere would tend to slow the spin of the sphere and also to align the spin with the field. Hence we would expect the spinning hole to line up gradually with the magnetic field and the entropy of the black hole to be increased by the Joule heating due to the stretched-horizon currents. This result was conjectured by Press[39] and proven by King and Lasota[40] and interpreted in terms of horizon currents by Damour.[9]

The interaction of rotating holes with electromagnetic fields is treated in considerable detail in other papers of our series: paper II (MT) and the review paper[18] which our group is now writing.

This paper has tried to motivate the adoption of the membrane viewpoint not only as a calculational tool in solving problems, but also as an aid to intuition in thinking about these problems. As was emphasized above, there is no difference in the physical predictions of the membrane viewpoint and other viewpoints; they are both consequences of general relativity and are thus mathematically equivalent. They differ solely in the aspects of the physics which they emphasize and in the array of mental pictures they present as aids to intuitive understanding of physical problems. This paper has attempted to show that, for problems involving dynamical electromagnetic fields around black holes, the mental pictures conjured up by the membrane viewpoint are much more apt for a physical description of the problem than are those conjured up by older viewpoints of black-hole horizons.

ACKNOWLEDGMENTS

We are indebted to Kip S. Thorne for many helpful suggestions during the course of this work and the preparation of the manuscript. We also thank the other members of the Caltech Paradigm Society: Richard Price, Thibaut Damour, Ronald Crowley, Wojciech Zurek, Ian Redmount, Sam Finn, and Xiao-He Zhang. This work was supported by the National Science Foundation under Grant No. AST82-14126.

APPENDIX

For a point particle of charge Q and mass m moving in flat space with four-velocity u^μ, the equations of motion including radiation reaction are[41]

$$F^\mu_{\rm ext} \equiv \frac{Dp^\mu}{ds} = ma^\mu - \tfrac{2}{3}Q^2(\dot{a}^\mu - u^\mu a^\nu a_\nu) , \tag{A1}$$

where $F^\mu_{\rm ext}$ is the external four-force, p^μ is the total four-momentum of the particle and its electromagnetic field, $a^\mu = Du^\mu/ds$ is the four-acceleration, and the overhead dot indicates differentiation with respect to the charge's proper time s. Since Eq. (A1) is generally covariant, it must be valid in Rindler coordinates. We choose kinematic quantities appropriate to a charge moving with constant ZAMO-measured velocity $d\mathbf{x}/d\tau = \beta \mathbf{e}_x$:

$$u^\mu = (\gamma/\alpha_0, \gamma\beta, 0, 0) ,$$
$$a^\mu = (0, 0, 0, g_H\gamma^2/\alpha_0) ,$$
$$\dot{a}^\mu = (g_H^2\gamma^3/\alpha_0^3, 0, 0, 0) ,$$

where $\gamma \equiv (1-\beta^2)^{-1/2}$, and where α_0 is the value of the lapse function at the position of the particle. When converted to a "per unit universal time" basis, $d/dt = (\alpha_0/\gamma)d/ds$, the rate of change of the x momentum of particle plus field as computed from Eq. (A1) is

$$\frac{dp^x}{dt} = \frac{\alpha_0}{\gamma}\frac{dp^x}{ds} = \frac{\alpha_0}{\gamma}F^x = \tfrac{2}{3}Q^2 g_H^2 \frac{\gamma^4\beta}{\alpha_0} ; \tag{A2}$$

and the rate of change of "energy at infinity" $-p_t$ of particle plus field is

$$\frac{-dp_t}{dt} = -\frac{\alpha_0}{\gamma}\frac{dp_t}{ds} = \frac{\alpha_0^3}{\gamma}\frac{dp^t}{ds} = \frac{\alpha_0^3}{\gamma}F^t = \tfrac{2}{3}Q^2 g_H^2 \gamma^4\beta^2 . \tag{A3}$$

By conservation of momentum, Eq. (A2) gives the rate of flow of x momentum into the horizon, and the corresponding rate of flow of angular momentum into the horizon is

$$\frac{dJ}{dt}=(2M\sin\theta_0)\frac{dp^x}{dt}=(2M\sin\theta_0)\frac{2}{3}\frac{Q^2g_H^2}{\alpha_0}\gamma^4\beta \quad \text{(A4)}$$

[Eq. (3.29)]. By conservation of energy at infinity, $-dp_t/dt$ is the rate of flow of energy at infinity into the horizon, i.e., the rate of increase dM/dt of the hole's mass [Eq. (3.26)]. The results derived here agree with the results obtained from explicit evaluation of the surface integrals (3.25) and (3.28).

[1]J. D. Bekenstein, Ph.D. thesis, Princeton University, 1972.
[2]S. W. Hawking, Commun. Math. Phys. **25**, 152 (1972).
[3]S. W. Hawking and J. B. Hartle, Commun. Math. Phys. **27**, 283 (1972).
[4]J. D. Bekenstein, Phys. Rev. D **7**, 2333 (1973).
[5]S. W. Hawking, Commun. Math. Phys. **43**, 199 (1975).
[6]J. B. Hartle, Phys. Rev. D **8**, 1010 (1973).
[7]J. B. Hartle, Phys. Rev. D **9**, 2749 (1974).
[8]R. L. Znajek, Mon. Not. R. Astron. Soc. **185**, 833 (1978).
[9]T. Damour, Phys. Rev. D **18**, 3598 (1978).
[10]T. Damour, in *Proceedings of the Second Marcel Grossman Meeting on General Relativity,* edited by R. Ruffini (North-Holland, Amsterdam, 1982); also for more detail, T. Damour, thèse de doctorat d'état (Ph.D. thesis), l'Université Pierre et Marie Curie, Paris, 1979.
[11]C. W. Misner, K. S. Thorne, and J. A. Wheeler, *Gravitation* (Freeman, San Francisco, 1973); cited in text as MTW.
[12]*Black Holes,* edited by C. DeWitt and B. DeWitt (Gordon and Breach, New York, 1973).
[13]K. S. Thorne and D. A. Macdonald, Mon. Not. R. Astron. Soc. **198**, 339 (1982); cited in text as TM.
[14]D. A. Macdonald and K. S. Thorne, Mon. Not. R. Astron. Soc. **198**, 345 (1982); cited in text as MT.
[15]R. D. Blandford and R. L. Znajek, Mon. Not. R. Astron. Soc. **179**, 433 (1977).
[16]R. H. Price and K. S. Thorne, in preparation.
[17]W.-M. Suen, R. H. Price, and I. H. Redmount, in preparation.
[18]K. S. Thorne, R. H. Price, W.-M. Suen, D. A. Macdonald, I. H. Redmount, R. J. Crowley, and X.-H. Zhang, in preparation.
[19]W. Rindler, Am. J. Phys. **34**, 1174 (1966).
[20]J. M. Bardeen, W. H. Press, and S. A. Teukolsky, Astrophys. J. **178**, 347 (1973).
[21]B. Carter, in *General Relativity, An Einstein Centenary Survey,* edited by S. W. Hawking and W. Israel (Cambridge University Press, Cambridge, 1979).
[22]D. Christodoulou and R. Ruffini, in *Black Holes,* edited by C. DeWitt and B. DeWitt (Gordon and Breach, New York, 1973).
[23]J. M. Bardeen, B. Carter, and S. W. Hawking, Commun. Math. Phys. **31**, 161 (1973).
[24]B. S. DeWitt and R. W. Brehme, Ann. Phys. (N.Y.) **9**, 220 (1960).
[25]A. G. Smith and C. M. Will, Phys. Rev. D **22**, 1276 (1980).
[26]W. G. Unruh, Phys. Rev. D **14**, 870 (1976).
[27]See, for example, J. D. Jackson, *Classical Electrodynamics,* 2nd ed. (Wiley, New York, 1975).
[28]T. C. Bradbury, Ann. Phys. (N.Y.) **19**, 323 (1962); D. G. Boulware, *ibid.* **124**, 169 (1980); M. Soffel, B. Müller, and W. Greiner, Gen. Relativ. Gravit. **12**, 287 (1980).
[29]R. S. Hanni and R. Ruffini, Phys. Rev. D **8**, 3259 (1973).
[30]E. T. Copson, Proc. R. Soc. London **A118**, 184 (1928); B. Linet, J. Phys. A **9**, 1081 (1976).
[31]T. Regge and J. A. Wheeler, Phys. Rev. **108**, 1063 (1957).
[32]R. M. Wald, Phys. Rev. D **10**, 1680 (1974).
[33]R. S. Hanni and R. Ruffini, Lett. Nuovo Cimento **15**, 189 (1976).
[34]See, for example, T. G. Cowling, *Magnetohydrodynamics* (Interscience, New York, 1957).
[35]W. H. Press, Astrophys. J. **170**, L105 (1971).
[36]C. J. Goebel, Astrophys. J. **172**, L95 (1972).
[37]A. R. King, J. P. Lasota, and W. Kundt, Phys. Rev. D **12**, 3037 (1975).
[38]E. S. Phinney, in *Proceedings of the Torino Workshop on Astrophysical Jets,* edited by A. Ferrari and A. G. Pacholczyk (Reidel, Dordrecht, 1983).
[39]W. H. Press, Astrophys. J. **175**, 243 (1972).
[40]A. R. King and J. P. Lasota, Astron. Astrophys. **58**, 175 (1977).
[41]P. A. M. Dirac, Proc. R. Soc. London **A167**, 148 (1938); also problem 17.4 of Ref. 27.